Feature Based Registration of Ultrasound and CT Data of a Scaphoid

by

Brian Oliver Koslowski

A thesis submitted to the
School of Computing
in conformity with the requirements for
the degree of Master of Science

Queen's University
Kingston, Ontario, Canada
May 2010

Copyright © Brian Oliver Koslowski, 2010

Abstract

Computer assisted surgery uses a collection of different techniques including but not limited to: CT-guided, fluoroscopy-guided, and ultrasound-guided imaging which allows medical staff to view bony anatomy of a patient in relation to surgical tools on a computer screen. By providing this visual data to surgeons less invasive surgeries can be performed on a patient's fractured scaphoid. The data required for a surgeon to perform a minimally invasive surgery while looking only at a computer screen, and not directly at a patient's anatomy, will be provided by CT and ultrasound data. We will discuss how ultrasound and CT data can be used together to allow a minimally invasive surgery of the scaphoid to be performed.

In this thesis we will explore two techniques of registering segmented ultrasound images to CT data; an Iterative Closest Point (ICP) approach, and an Unscented Kalman Filter-based Registration (UKF). We use two different ultrasound segmentation methods; a semi-automatic segmentation, and a Bayesian segmentation technique. The segmented ultrasound data is then registered to a CT volume. The success or failure of the registrations is measured by the error calculated in mapping the corresponding land- marks to one another and calculating the target registration error. The results show that the Unscented Kalman Filter-based registration using the Bayesian segmentation of ultrasound images has the least registration error, and

has the most robustness to error in initial alignment of the two data sets.

Acknowledgments

There are many people I need to thank for the success of me completing this thesis. First I must thank my wonderful wife Hillary, she's the one who kept me going on those nights when the last thing I wanted to do was be awake writing. My parents John and Renate for their continuing support and encouragement regardless of how many times I was "almost done writing." In the same way I must thank Janis and Fernando for allowing their daughter to marry a professional student. Last but not least is Chris Riddle whom I must thank for all his help throughout this process. I love you all very much and this thesis is as much for you as it is for me.

I also must send many thanks to my lab mates, Thomas and Mehdi have provided me with much insight and information that made it possible for me to tackle the topics covered between the covers of this book. Many thanks go out to Maarten and Kathrin for their help as well. And most importantly Dr. Purang Abolmaesumi for his guidance and patience helping me get through this.

Of course I'd also like to thank all my friends including but not limited to: Bob Faser, Matt Kirky, Marty Matusiak, Dan Yau, Jason Gomori, the Sodoku Club, the Blue Screens, and all the rest.

Contents

List of Tables

List of Figures

Chapter 1

Introduction

1.1 Motivation

As the number of techniques for creating more accurate image-guided systems increases, the need to evaluate how successful these techniques are within particular scenarios arises. Within the context of this thesis, the application of percutaneously pinning a fractured scaphoid bone under the guidance of ultrasound imagery is the primary means of evaluation. Existing techniques for repairing scaphoid fractures involve open surgery of the wrist where a surgeon exposes the anatomy in order to perform the re-unionization of the scaphoid. That said, there is a less invasive surgery that utilizes fluoroscopic guidance to track the placement of a pin beneath the surface of the skin via a monitor.

The motivation of this thesis is to move to a minimally invasive computer assisted surgery technique that provides the patient with a shorter recovery period, a higher probability of bone union, and a lower chance of complications in the operating room (hereinafter OR). The goal of computer assisted surgery is to provide a method by

which a trained surgeon can obtain real-time feedback of what is occurring subcutaneously (beneath the surface of the skin) from a video screen. By displaying the surgeon's tools in relation to the patient's anatomical structures on a screen, the patient's anatomy does not need to be directly exposed to the surgeon. The tools are tracked with a camera tracking system while the patient's anatomy is viewed by ultrasound sonography. Systems that use computers in the OR to display anatomy and/or track tools are know as Computer Assisted (Orthopedic) Surgery (hereinafter CA[O]S) systems. CAS's are often utilized to minimize the invasiveness of a procedure while decreasing the healing time by decreasing the invasiveness of a procedure. This is accomplished by creating a virtual representation of the patient to show the progress of the surgery, thereby avoiding the invasiveness of an open surgery.

Current CAS systems contain a bottleneck in the segmentation, being preformed manually to ensure accuracy, to ensure accuracy. This is the step where it is believed to be room for improvement [SKJT05]. By eliminating the manual segmentation, or using a technique that does not require ultrasound images to be segmented, there can be an increase in speed over methods that use segmented data; take [BM] [Yan] [HA06] [PMV03] [FWD04] [BER$^+$02] [HDM$^+$98] for example. A method described in [SKJT05] [JT04] offers an approach that uses an ultrasound to computed tomography (hereinafter CT) registration without manually segmenting the ultrasound image by using a probabilistic Bayesian framework.

There is a need to explore how a coupling of a probabilistic approach with a conventional registration technique can positively influence the speed and accuracy of image-guided percutaneous pinning procedures. Therefore the purpose of this thesis is to compare both semi-automatic segmentation and probabilistic segmentation

when coupled with Unscented Kalman Filtering (hereinafter UKF) based registration and Iterative Closest Point (hereinafter ICP) registration to determine the most accurate combination of segmentation and registration techniques. The accuracy of the techniques will be determined by calculating the target registration error of the segmentation and registration tests.

Prior to discussing the findings of this study, a review of current methods used in image guided surgery may be helpful. It is pertinent to examine CT-guided surgeries, X-ray and fluoroscopy based methods, and finally, ultrasound-guided techniques. This examination will be followed by a study comparing the effectiveness of semi-automatic manual segmentation and probabilistic segmentation of ultrasound image. I will use the segmented data to register the ultrasound images to a 3D model of their corresponding anatomy (in this case the scaphoid bone) by employing two different techniques: Unscented Kalman Filter [HA06] and Iterative Closest Point [BM]. Finally, the target registration error (hereinafter TRE) of both registrations techniques will enable us to arrive at a conclusion concerning which technique performed best in the tests. If the findings show there can be an increase in the speed of CAS-system without any loss of accuracy (or ostensibly those traits viewed as desirable while performing a successful surgery of the wrist), there is reason to believe that utilizing minimally segmented data is a desirable modification to the current methods.

In order to solve the aforementioned problem of utilizing minimally segmented data we can use either methods of semi- or fully-automatic ultrasound image segmentation. Some examples of techniques that successfully segment a hip or spinal bone in an ultrasound image are presented in [VdBA+04] [BER+02] [HDM+98]. However, due to the unique shape of the hip and spinal bones used in these studies, it

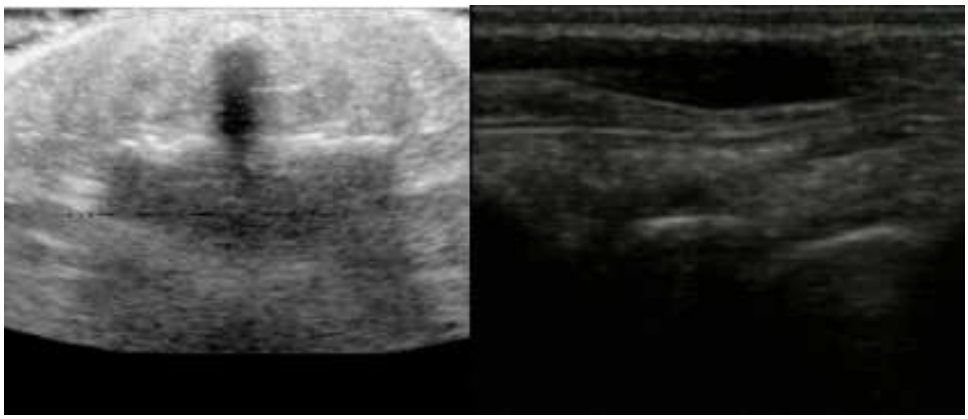

Figure 1.1: A spinal ultrasound image, show on the left, contains sharp peaks which define the bone surface, whereas the scaphoid, shown on the right, has a much rounder and softer response thus making it more difficult to segment.

is difficult to adapt these algorithms to the scaphoid bone. Due to the sharp edges of vertebrae, it is much simpler to segment these images since the bone's surface is highly pronounced, as shown in Figure 1.1.

In contrast, it is difficult to accurately identify the scaphoid's surface in the image. It stands to reason that extracting the surface will be equally difficult when employing automatic segmentation algorithms. Manual segmentation offers a solution by utilizing knowledge of the anatomy to perform a high quality segmentation. The quality of this segmentation comes at the cost of time, thus rendering this method unacceptable for use in real-time applications in the OR. There are also some semi-automatic techniques [AB94] where a user selects a small region of seed points that grow until the data is segmented. This to is too time consuming for use in the OR as it requires user input on each independent image.

Another suggested solution is to switch from a method that uses binary-segmented images, to one that utilizes processed images to show the probability of a specific

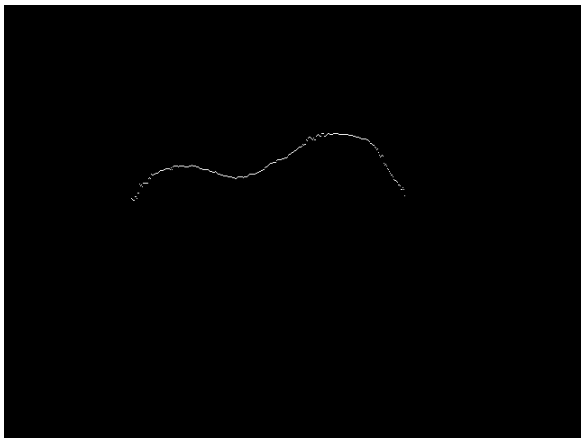

Figure 1.2: This shows a probability image that instead of being segmented fully contains pixel values which correspond to the likelihood that a specific pixel lies on the bones' surface.

pixel laying on the surface of the bone [SKJT05]. Within this theory, a feature-based method is coupled with a probabilistic network that manipulates the image from an eight-bit gray scale image to a probability matrix in which the highest probability refers to the strongest surface estimation. A network of features is applied to both the ultrasound images and the CT slices, after which the resulting probabilistic (see Figure 1.2) images are registered to one another. Since the feature-based algorithm can be applied fully-automatically once the required parameters that define a region of interest have been entered, this enables us to eliminate the human-dependence from the process. From this we can infer that probabilistic images can be employed as a plausible solution to the aforementioned problems when using CAS systems in the OR.

1.2 Percutaneous Pinning of the Scaphoid

Percutaneous pinning is a unique computer assisted surgery in which a pin is placed percutaneously, through the skin, to repair a non-union fracture eliminating the need for a highly invasive surgery. Entry into the patient consists solely of an entry wound from a drill. The technique of percutaneous scaphoid pinning involves a pin, also known as a screw, being placed through a small hole drilled through the skin and scaphoid. Using image-guidance gives the surgeon a real-time virtual (on-screen) environment showing the position of his or her instruments below the surface of the skin in relation to the fractured scaphoid bone. A computer and cameras constantly track the tools position in real space while converting their position to virtual space on the computer screen.

Numerous common difficulties with the conventional method of repairing a fractured scaphoid are discussed in [RN03][1]. Percutaneous pinning differs from the previous methods insofar as it allows for a greater chance for unionization to occur. It is not without it's difficulties and requires a method whereby the process of the surgery may be accurately tracked. In order for correct tracking (therefore also visualization) of the tools to occur, one must rely upon the usage of one or more of the following multi-modal imaging techniques: radiography, fluoroscopy, computed tomography (hereinafter CT), and magnetic resonance imaging (hereinafter MRI) [Sug03]. A tremendous amount of research focuses on the topic of percutaneous pinning: [TCB+01] [CTL+98] [CTMT00]. That said, [ALA01] [YWCS02] and [MH03] explicitly address the fixation of wrist bones by means of percutaneous pinning.

[1]To give the reader a good understanding of conventional wrist fixation and scaphoid fractures, [RN03] is a great source. It gives a thorough basis of wrist anatomy and the difficulties of detecting and treating scaphoid fractures.

Due to the twisted shape and orientation of both the scaphoid bone as well as it's small nutrient supplying blood vessel, it is imperative to quickly detect and repair the fracture. If the fracture is not detected prior to the blood supply to the scaphoid being diminished avascular necrosis (death of the bone) can occur. This occurs because the scaphoid bone has a limited blood supply from the radial artery and anterior interosseous arteries. In order for bones to reunify, an abundant supply of blood must be present. As there is such a low blood flow to the scaphoid while immobilized by a cast, there is the possible occurrence of a non-union. To increase the chances of a union, the bone fragments are often joined by screwing the two halves together.

A fracture known as a "Puncher's fracture" [RN03], the most common type of fracture in the wrist, can result from falling on an out-stretched hand or from a direct strike while the hand is balled into a fist; see Figure 1.3.

The symptoms of an injury like this include, but are not limited to, tenderness in the anatomic snuff box, swollen wrist joint, numbness of the thumb, and general pain in the wrist and hand. These symptoms are also common to a sprain in the wrist, therefore increasing the likelihood of a fracture going untreated for quite some time until a correct diagnosis can be made. Once a fracture has been discovered, the choice of immobilization technique (either placing the wrist in a splint, casting, or surgery) often lies with the surgeon.

Of the various options for surgery, percultaneous pinning offers the greatest probability of a wrist healing successfully. The advantages of percutaneous pinning over cast immobilization, a method not addressed in [RN03], are examined in [ALA01]. Adolfsson conducted a study of 53 patients with undisplaced fractures of the wrist, where the fractures were either transverse or oblique (the fracture occurred across

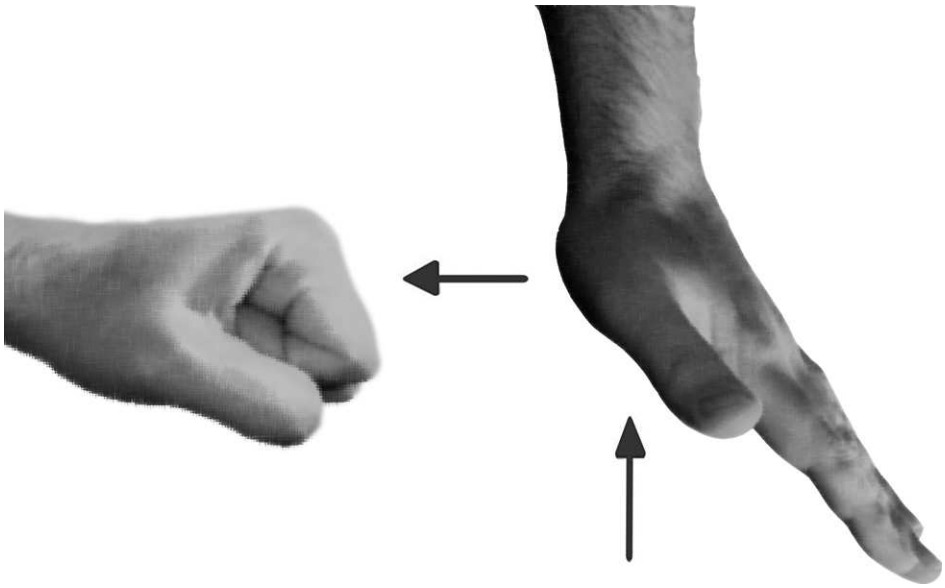

Figure 1.3: Shown are the two different forces which can cause an undisplaced scaphoid facture. On the left is a puncher's fracture and the right shows an outstreched hand fall. The arrows represent the direction the force is applied to cause the fracture.

the narrow area of the bone). Of these two groups, the first received a cast that immobilized the arm from the elbow to the wrist. The second received surgery to unionize the fractured pieces of the scaphoid. Post surgery, the second group wore removable plastic splints that extended from their wrists to their hands.

The results in [ALA01] concluded that the early mobilization allowed by the pinning of the wrist helped the patients regain greater use and movement, therefore resulting in a more mobile wrist over the wrist immobilization group. Pinning tends to also be a more reliable method of holding the bone fragments together as there is less chance of avascular necrosis occurring, often cited as the primary fear of casting a wrist for a scaphoid fracture [ALA01] [RN03].

1.3 Image-Guided Surgery

Recent research trends in image-guided surgery include, but are not limited to; endoscopic navigation, neurosurgery by Magnetic Resonance Imaging (MRI), and 3D modeling of anatomy for surgical planning. These trends rely upon medical image segmentation, and multi-modal image registration, which this thesis focuses on. Of particular interest is the segmentation and registration areas of the field; including ultrasound to CT registration, with additional focus ultrasound-guided and fluoroscopy-guided surgery.

CT-based guidance covers a broad research area. From mental registration, where the surgeon would visually inspect a 3D model or individual CT slices and cognitively plan the surgery, to tracking a bone by attaching device directly to the bone to track its position. By attaching trackers, the view of the anatomy is not hampered by blood and tissue that a conventional surgeon, one who is cutting the patient open to expose the anatomy, would be burdened with. However, there is a downside to mounting tracking tools directly to the bone. Such procedures are intrusive, as trackers need to be rigidly attached to the bone's surface by screws. While this method may lend itself to effective techniques involving larger bones such as the tibia or hip as there is substantial surface area and rigidity to support a dynamic reference base (hereinafter DRB), this is not a viable method for surgeries involving the wrist, as mounting the tracker would further damage the scaphoid bone.

J. Tonetti examine the benefits as well as the difficulties associated with the percutaneous pinning of a hip [CTMT00]. Similar to [ALA01], Tonetti's study ultimately arrives at the conclusion that the advantages of a reduced invasiveness procedure

over conventional surgery outweigh the negative aspects. Percutaneous pinning performed with fluoroscopy guidance is argued to be a successful technique. However, it is noted that because the technique is delicate [TCB+01] a well trained operator is required. Instead of using fluoroscopic images, an ultrasound guided method can also be used [BPA+05] [CBEP05]. By displaying a 3D surface model generated from CT images on a monitor as the reference image of the region of interest, and updating the orientation of the model with ultrasound based registration, we can provide a surgeon with a virtual view of what is happening beneath the surface of the skin. An important advantage of an ultrasound guided CAS is its radiation-free image acquisition. When utilizing this method, the patient as well as the surgeon, are not exposed to radiation during the operation. Patient discomfort was noted as being the same in a post-operative interview stating that "[the] pain evaluation, drug consumption is similar in both groups." [TCB+01] In conclusion, the ultrasound-guided CAS procedure described in the paper for percutaneous screwing of the posterior lesion of pelvic ring fractures is a safe and accurate alternative to fluoroscopic imaging, and is also a safer method for the surgeon in so far as it eliminates exposure to large amounts of ionizing radiation.

1.4 Objective

This thesis aims to evaluate the feasibility of using ultrasound imaging in computer-assisted orthopaedic surgery. Here, we use the computer-assisted fixation of scaphoid fractures as a test-case. In this surgery, accurate alignment of ultrasound and CT data plays the key role to the success of the ultrasound-guided approach. Hence, in this thesis, we evaluate two different methods of registering ultrasound images to CT

data sets. The first method involves the manual segmentation of ultrasound images, whereas in the second approach, we use a Fast Algorithm for Probabilistic Bone Edge Detection (hereinafter FAPBED) [SKJT05] to segment the ultrasound data. We will compare the performance of registration of two feature-based registration techniques, Iterative Closest Point (ICP) [BM] and Unscented Kalman Filter-based registration [HA06]. The success of the registrations will be measured by the target registration error between corresponding landmarks identified in CT and ultrasound data.

1.5 Contributions

In this thesis, I have:

• compared the performance of two feature-based registration techniques, i.e., ICP and UKF, for aligning ultrasound and CT data sets. The comparison has been based on the time of convergence, registration success rate and the value of final TRE.

• demonstrated that using a Bayesian segmentation of ultrasound data, one could obtain lower registration errors than a semi-automatic binary segmentation of ultrasound data.

• developed a visualization program to simultaneously display ultrasound and CT data sets. The program could be used to provide an initial manual alignment of ultrasound and CT data.

1.6 Thesis Outline

The thesis is divided into five chapters that present the segmentation methods, registration methods, describe the experimental set up and discuss the results of the experiments. This thesis is organized as follows:

Chapter 2 Segmentation: presents prior work in CT and US segmentation techniques. Then I explain and expand on the FAPBED segmentation methods and show resulting data from running this segmentation on experimental data.

Chapter 3 Registration: presents a background of current registration techniques including: manual, statistical shape model, and maximum intensity. Then there is a more in depth look at the two registration techniques used in this thesis; Iterative Closest Point and Unscented Kalman Filtering-based registration.

Chapter 4 Experiments and Results: presents the experimental design and the registration results of the experiments. There's a discussion of the results where the results of the experiments are shown.

Chapter 5 Conclusion and Future Work: presents the conclusions of my thesis and areas of future work that can aid in expanding the experiments from Chapter 4 using clinical data rather than phantom models used for this thesis' experiments.

Chapter 2

Segmentation

In order to efficiently use ultrasound imaging as a form of guidance in the operating room, all superfluous data must be removed from the image. This process is known as segmenting an image. In the following chapter, the benefits and challenges of using B-mode ultrasound, and other modalities, as a guidance technique for minimally invasive surgery, or CAS , will be discussed. In Section 2.1 the challenges and solutions to these problems will be addressed, followed by an examination of an ultrasound segmentation technique that uses a "feature-based algorithm" to segment the bone surface from the ultrasound images. These segmented slices are then used to compute transformation parameters to map the ultrasound images to a matching CT surface model [JT04]. This technique will be compared to a "Maximum Intensity" technique through a demonstration of the advantages and disadvantages of the segmentation methods. In order to register sets of data to one another, it is ideal to have both the CT (or the fixed data set), as well as the ultrasound image (or the the moving data set), segmented. As the fixed image model, in this case acquired preoperatively, must also be segmented, this raises another challenge that must be addressed in this chapter.

Section 2.4 will address the FAPBED algorithm [SKJT05] for semi-automatically segmenting the CT data.

2.1 Ultrasound Segmentation

The primary focus of this section is the examination of a "feature-based segmentation" technique that converts raw ultrasound images into probability maps. The probability map is in the form of a Bayesian probability, where the pixel is either on the bone's surface or not, allowing for a simple transformation to an image showing the probability of a pixel being on the surface.

This will be compared to a simple but effective, "maximum intensity segmentation" algorithm, that works on the basis that the brightest pixels in an image, or the highest intensity response, are the ones that must correspond to the bone surfaces in the image. The feature based technique is one that was introduced by Ameet Kumar Jain in [JT04].

Jain et al. [JT04] take an approach to segmenting ultrasound that is quite different from those techniques previouslyu discussed. The first crucial difference is that Jain's group argued that in order to effectively find the bone in ultrasound scans, one must first develop an understanding of the underlying physics behind B-Mode ultrasound bone responses. Moving forward the primary findings of [JT04] were that as the ultrasound beam left the transducer and has a teardrop shape that is much different than the previously assumed constant and planar shape. This confirmed the finding that the surface of the bone in the response was not on the surface of the curve, but rather within the response band (this is shown in Figure 2.1). Therefore, as the angle of incidence deceases from the surface normal of the bone, the location of the

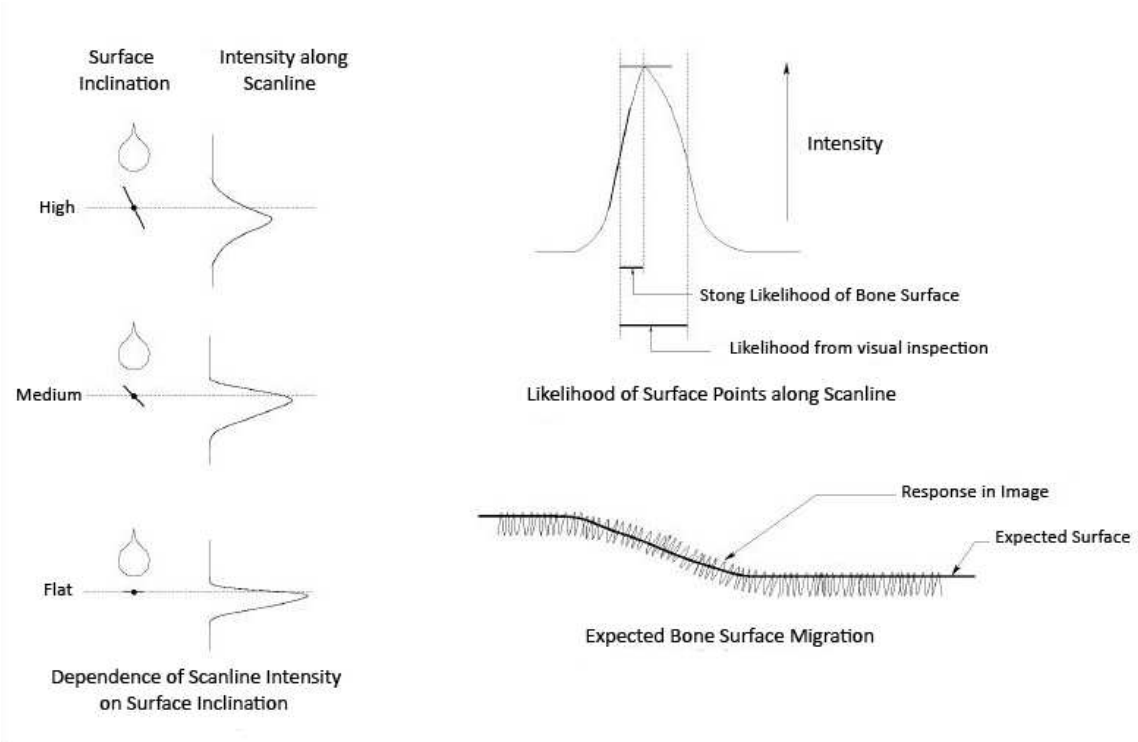

Figure 2.1: This image shows the expected bone surface response from an ultrasound and the actual bone's surface position in an ultrasound scan. Used with permission from Amit Jain [JT04]

surface within the ultrasound image actually moves inside of the band. This was discovered by using fiducials and determining that the response from the bone was directly correlated to the angle of incidence of the ultrasound beam. As the angle of incidence deviates from the surface normal of the bone at the point of intersection, the position of the bone surface within the bone's response is beneath the top of the band. Also, the greater the deviation from the surface normal, the greater number of pixels there are between where the bone's surface is shown in the image, and the actual location of the bone in real space.

Using this knowledge, [JT04] was able to devise a feature-based algorithm more successful at segmenting ultrasound images. To start, a straight forward median filter

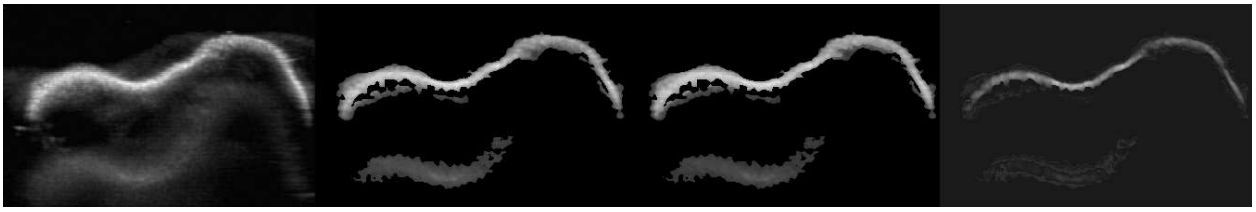

Figure 2.2: On the left is the original image containing all the information from the ultrasound scan, the centre ones show the intermediate steps, and the right image shows partially segmented data previous to the final segmentation from the feature-based segmentation.

is employed to clean the image of speckle and background noise. Second, a threshold algorithm is used to determine if the image contains a true bone surface or just an artifact. If a threshold value (determined by the user), is not reached, then the image is labeled as an artifact. The final preprocessing step is one that removes a high-intensity band at the top of the image where the transducer comes into contact with the skin. If not removed, it could cause a false bone surface to be detected as it may have similar intensity to that of bone. After preprocessing the image, the bone surface is segmented by extracting five features from the image. An example of these different features can be seen in Figure 2.2.

Feature one is an intensity measure, involving the maximum intensity segmentation discussed above. Feature two involves a high intensity gradient that targets areas that contain bone and other high contrast positions. The third feature looks along each scanline (each column of pixels) for a "specific shape of the intensity-profile along a scanline" [JT04]. This can be described as being a 7 pixel thick line which has a sudden rise in intensity on the front side and a slower slope on the backside. This shape has been modeled by joining two Gaussian curves together. The first half of the curve is a Gaussian curve with a standard deviation of 1, while the second half (which slopes back down from the top of the first curve) has a standard deviation of

2. While the next two features are not used to segment the images in this research they nevertheless require mentioning. The first is a shadow region in the image that occurs when a medium is encountered that does not allow for the ultrasound signal to penetrate through it. Secondly, there is a "multiple reflections" feature that has minimal effect when applied to the phantom images used. In some ultrasound images there can be multiple responses to a bone surface, because of different layers that the ultrasound bounces off of before getting back to the transducer, which results in a second, and sometimes even a third reflection. These different features can be calculated in any order, and theoretically, could all be performed in parallel to speed up the algorithm. Finally, the probabilistic framework must be formed to properly extract a segmentation, or a probabilistic image.

2.2 Segmentation of CT and US Data - Background

As previously mentioned, there are very few ultrasound-guidance systems that function without the ultrasound image being segmented prior to viewing. The process of segmentation involves extracting the bone surfaces from the CT or ultrasound images without losing any pertinent information. If ultrasound images are to ultimately be mapped on top of CT images, the segmentation must be accurate to ensure a correct convergence. Due to the nature of ultrasound imaging, segmentation can range from quite simple, in the case of a clean phantom image, to very difficult, in images of actual human anatomy. Ultrasound images, as shown in the right most image of Figure 2.3, contain multiple reflections, dark shadow regions, and different intensity responses to corresponding medium densities.

The CT images must also be segmented as they are taken by passing Xrays through

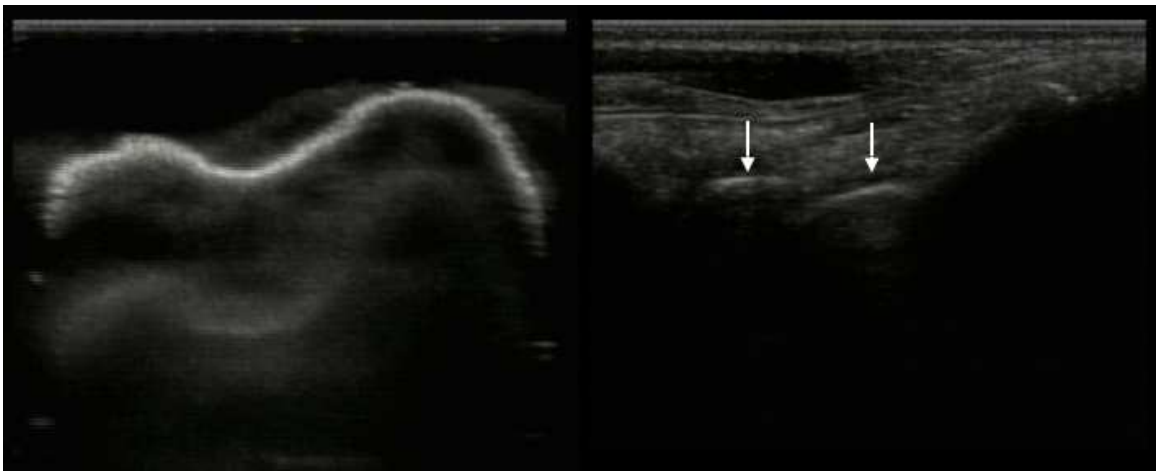

Figure 2.3: The difference between a clean phantom image on the left is compared to the noisier and harder to interpret image on the right. These images serve to show the difference between phantom images and images obtained in the OR.

a piece of anatomy. Since the bone is not the only anatomy which is captured by the Xray images, there is also extra information in CT data. This information is of softer surrounding tissue. Additionally, the table on which the anatomy is placed as well as any other artifacts which may be present on the patient (for example: fixation screws or surgical plates, if made from metal, can cause a spectral artifact) can negatively effect the quality of the information provided by Xrays.

There are some registration techniques that rely upon using ultrasound images that do not require segmentation [SKJT05]. This has the added advantage of reducing the likelihood of error from a faulty segmentation that could propagate causing the registration to fail. In addition, since manual segmentation of ultrasound is a fairly slow and difficult task, one can assume that a technique that does not rely upon segmentation will provide must faster results. That said, the challenges, advantages, and disadvantages of image registration [SKJT05] where segmentation of the

ultrasound images is not required will be discussed later in this chapter.

2.2.1 CT Segmentation

Basic DICoM viewers, Mesher, and image editing programs are just several of the many tools that allow for manual segmentation of CT data. Manually segmenting images relies upon the theory that the human eye is much better adapted at distinguishing between different regions of interest in the image. Additionally, manual segmentation has the strong point of being the simplest technique. With proper training there is a high probability of getting a correct segmentation. It has the downfall however, of being tremendously time consuming and tedious. In order to complete a proper segmentation, a vast knowledge of the anatomy is required. In addition to lending themselves to a higher probability of proper segmentation, manual segmentation techniques have also been used in the repairing of regions of interest that have been incorrectly segmented by an automated process.

A semi- or fully-automatic method which offers a good degree of segmentation, if not the most accurate, is thresholding the image. The method entails a value being chosen wherein all pixel values greater than the predetermined threshold value are accepted as being in the region of interest. All other pixels within the image are set to a value of zero, thereby indicating they are not the bone. The segmentation technique described above is referred to as global thresholding, as the same threshold value is used for the entire image. Because the density of the anatomy is non-uniform, the simple approach of using a single value can easily accept or reject erroneous pixels. There is a second form of thresholding that is a slightly more advanced variation. Local thresholding breaks the image into a smaller grid whereby each grid locations

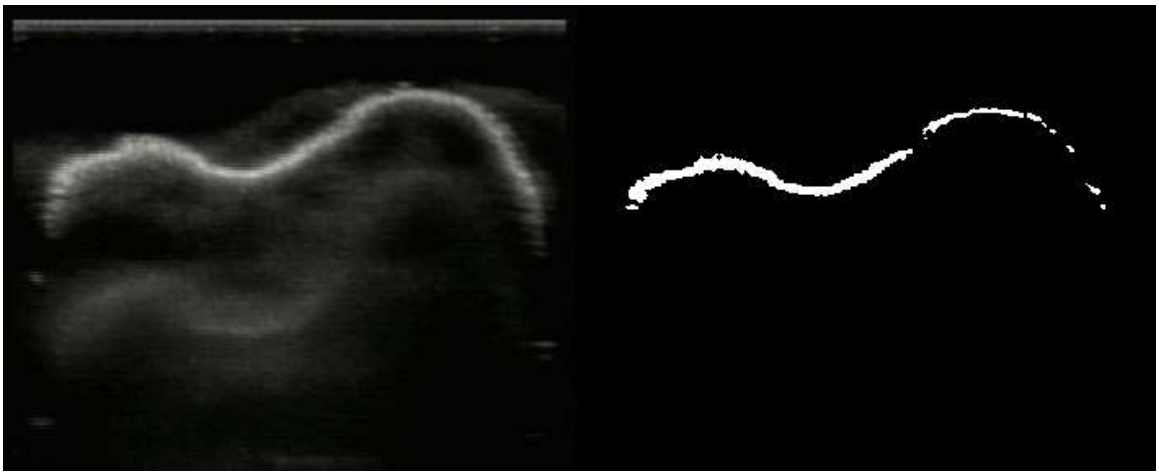

Figure 2.4: This shows the original image on the left and the segmentation of the image on the right using a global threshold segmentation. Note that there has been bone surface lost after the segmentation.

can be thresholded independently, allowing for a more robust segmentation.

Each of these threshold segmentation techniques has its own drawbacks and strong points which restrict their uses to the applicant's discretion. Global thresholding can lose vital pieces of the anatomy due to its naive true or false approach which does not account for variations of density in the anatomy. The localized approach however, can do the exact opposite by amalgamating neighboring regions which have similar densities but are not of the same region. As a stand-alone method of segmentation, these threshold methods offer little in the way of user assurance of a proper segmentation, but in conjunction with other methods they provide a good initial step to segmentation.

There are several tools which allow for manual segmentation of CT data sets. These include: basic DICOM viewers, Mesher, image editing programs, just to name a few. Manual segmentation has the strong point of being the simplest technique in that with proper training there is a high probability of getting a correct segmentation.

It has the downfall however, that it is extremely time consuming and tedious, and in order to get a satisfactory segmentation, a vast knowledge of the anatomy is required. A secondary use for manual segmentation can be to repair regions of interest that have been incorrectly segmented by an automated process.

Segmentation - Seeded Region Growing

Seeded Region Growing by Rolf Adams and Leanne Bischof [AB94] introduces a technique of segmentation that uses "local intensity data," rather than global thresholding techniques. The seeded region growing technique, as the name implies, is a region growing method with modifications to make it more robust. The algorithm itself is most easily explained by thinking of it as breaking an image into smaller components, a seed, and then running a threshold segmentation on each of the pixels neighboring the seed. If the neighbor is within a predetermined threshold then it is included in the segmentation and if not it is discarded. This process is repeated until none of the neighboring points are within the predetermined range. The seeded region growing technique works well in controlled situations (as outlined in [AB94]), which validates that the algorithm can work, however this implies that SRG may only work in this staged environment, but not necessarily in clinical application. A seeded region growing algorithm is shown in Figure 2.5.

2.3 CT Segmentation

CT images, while much higher in clarity than ultrasound images, also require segmentation. Where ultrasound images suffer from speckle noise, and other image defects discussed in Section 2.1, CT slices contain; soft tissue, secondary bony structures,

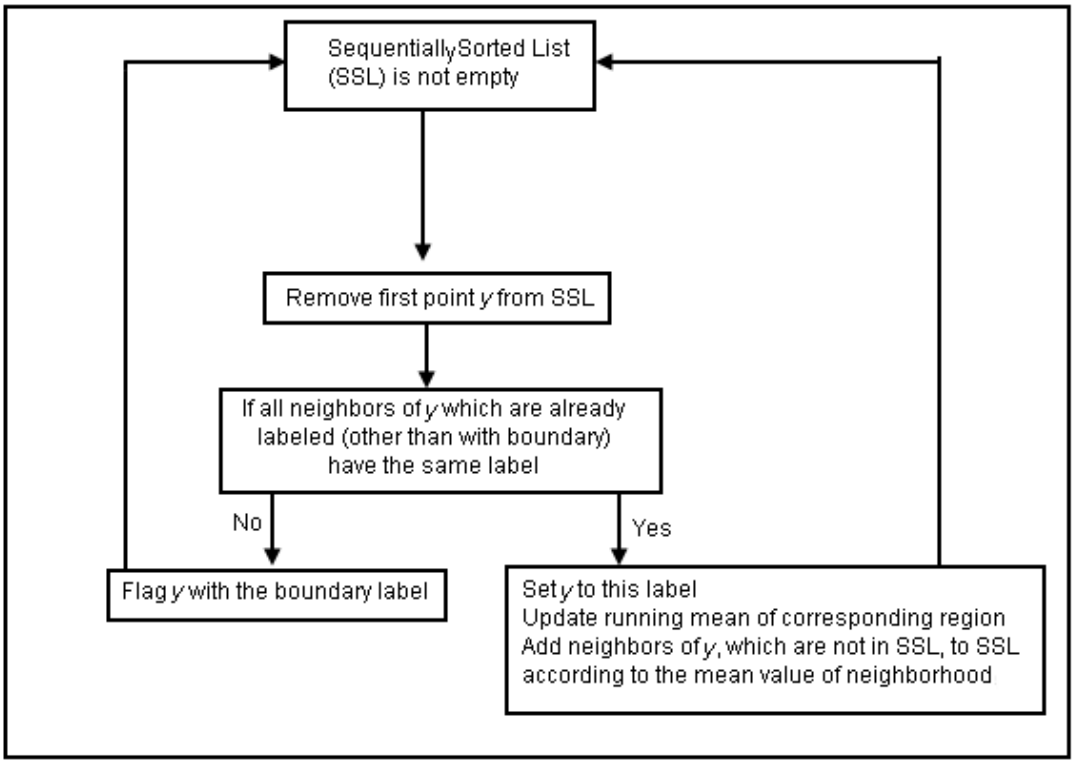

Figure 2.5: Outline of the Seeded Region Growing algorithm [AB94].

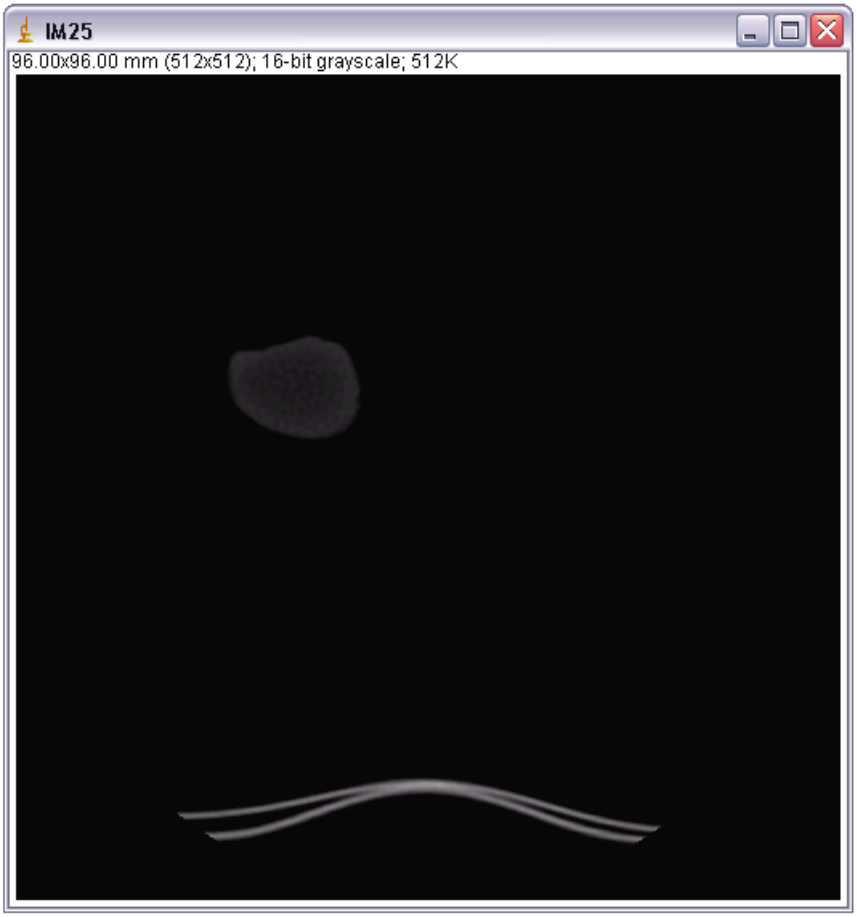

Figure 2.6: This unsegmented CT image clearly shows the bony structure, highest intensity in the image, but being unsegmented there is far too much extraneous information in this image to build a surface model of the bone.

and metal artifacts (in this case the device that holds the phantom bone during the CT scan), all of which need to be removed to segment the bone. As discussed, the methods used each have unique draw-backs. Therefore this section will focus on a manual segmentation program; Mesher, which is compared to the Fast Algorithm for Probabilistic Bone Edge Detection [SKJT05], a (semi-)automatic CT segmentation tool.

2.3.1 Segmentation with Mesher

Mesher is a tool developed at Queen's University to manually segment CT data slice-by-slice to build an accurate model. There are several different tools offered by Mesher to aid in the segmentation process. These tools can be seen in the lower right hand corner of the GUI and include; measure, paint, rubber band, zoom, threshold, and an apply to all slices button which semi-automates the process. The measure tool is useful for determining the exact size of anatomy and to aid in the identification of different features. That said, the most used tool in Mesher is the paint tool that allows the user to trace the outline of the region of interest and to subequently delete the unnecessary information, thus allowing for a cleaner and more accurate 3D model to be created.

The rubber band is used to get rid of a chunk of data separated by empty space. Within the present context, the CT data had two regions of high intensity in each slice, one was the phantom model, while the second was the device holding the model still during the CT scan. The threshold tool helps get rid of entire pieces of data that are within the same range of density. This is practical, as soft tissue is of a lower density than the surrounding bone and therefore eliminates the need to slowly paint away the soft tissue manually. Finally, there is the zoom tool to assist the segmentation process by allowing the user to enlarge the image and if necessary, edit pixel by pixel to increase the accuracy of the segmentation. There is also an option that lets user apply the same step to every slice that he or she desires. This option used in conjunction with the rubber band tool can quickly delete unneeded information.

The main disadvantages of using Mesher are that the accuracy of segmentation is

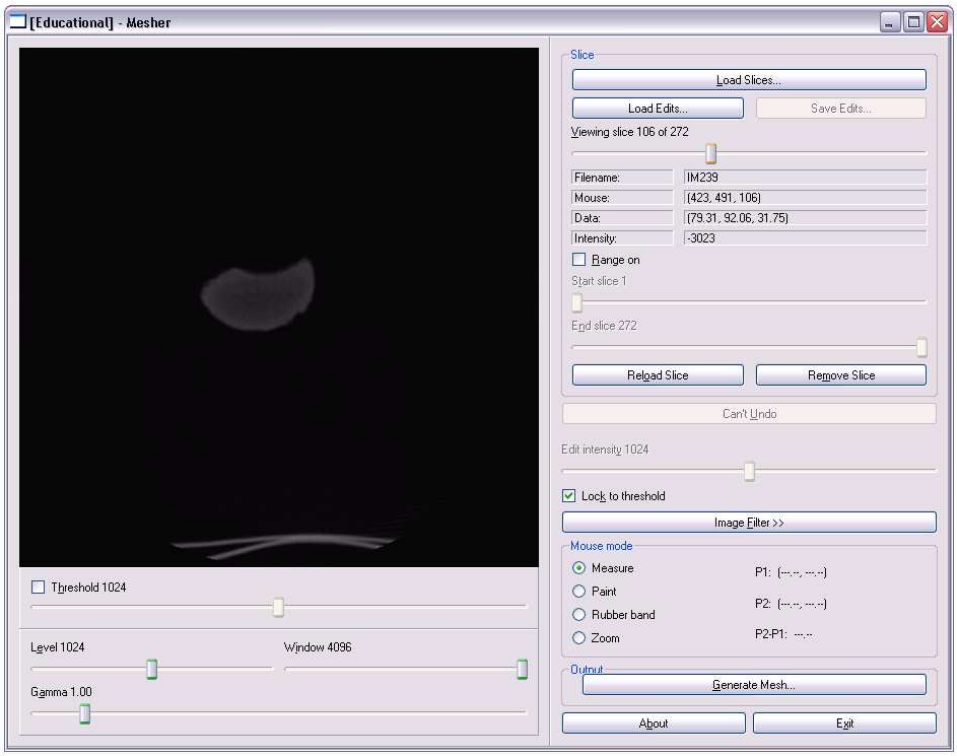

Figure 2.7: Mesher interface, showing all of the different tools available.

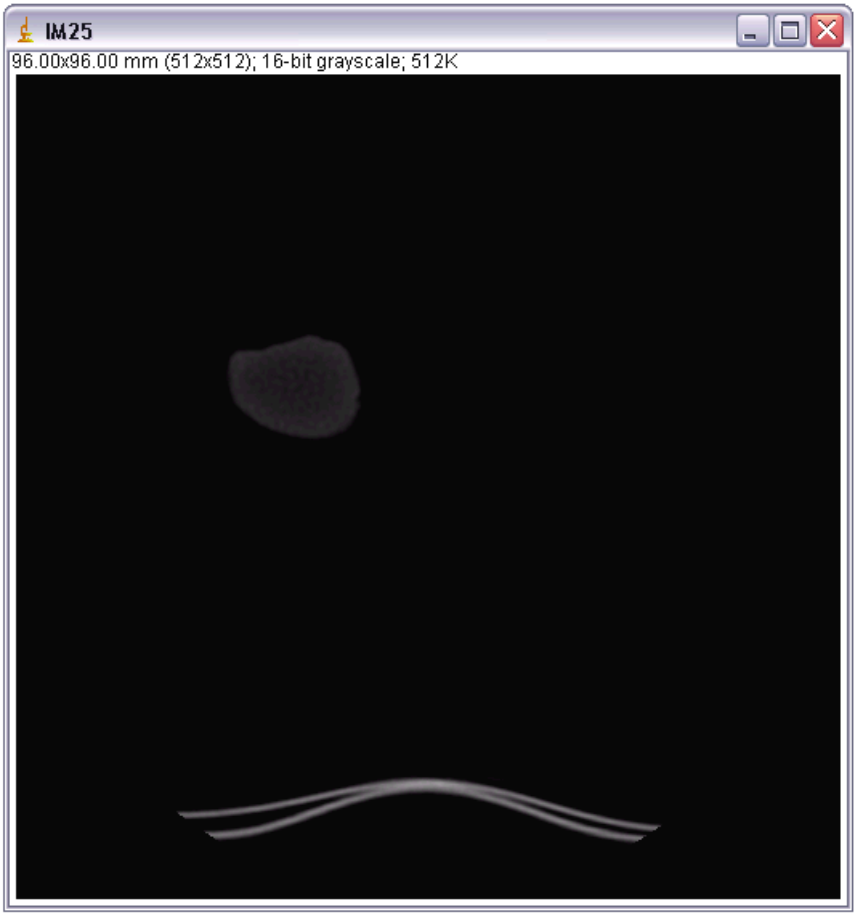

Figure 2.8: This image shows the two distinct regions in the CT scan which are separated by empty space. This high intensity region causes trouble for both manual segmentation and FAPBED.

directly related to the familiarity of the user with both Mesher and the anatomical shapes of the region of interest. If Mesher is used incorrectly, the resulting 3D mesh can be slightly deformed, and this coupled with an erroneous ultrasound segmentation can lead to the overall registration being affected in such a way that the information acquired is rendered unusable. Also if the user is untrained in Mesher, there is a slight learning curve causing the process to take slightly longer than with a trained operator. These however, can be considered minor setbacks, as the main flaw with Mesher is the shear amount of time required to do a segmentation for both beginners and fully trained users alike. Since this step is performed pre-operatively, the time required is less important than the resulting mesh, but the task is tedious and should in the very least, be upgraded to a semi-automatic, if not fully-automatic, technique.

2.4 Automatic Segmentation with FAPBED

To overcome the obstacles and tediousness of manually segmenting images, a semi-automatic solution, FAPBED [SKJT05], can be employed to segment data. As in [JT04], FAPBED is a "probabilistic framework that addresses the segmentation-registration duality, wherein exact segmentation is not a prerequisite..." [SKJT05]. FAPBED also uses features in a probabilistic Bayes' classifier. These features convert the data from Houndsfield Units (hereinafter HU) into a binary image (0,1), which can then be registered to the probabilistic ultrasound segmented volume. The feature extraction is run only after the images have gone through some preprocessing. In this case, the preprocessing may involve either a conservative or aggressive thresholding, as well as a volume limiting step to decrease the runtime.

By thresholding the image, approximately 96% of non-surface points and only

10% of surface points are eliminated. Additionally, thresholding reduces the speckle in an image while maintaining a high number of vital pixels [SKJT05]. The second time-reducing method is the volume limiting feature, which puts a window around the perimeter of the region of interest to reduce the size of the search area. The size of the image is reduced, on average, by 51%, or if using a more advanced volume limiting step, as high as 85%. The purpose of the aforementioned feature extraction steps, is to reduce the size of the region of interest to include only the bony surfaces. By doing so, the run-time of the program can be drastically decreased. Within this method there are five features used, each of which will be shown and analyzed below.

Density, the first feature, is defined as any bony anatomy appearing in the CT images between the range of 960 and 2493 HU as predetermined in [SKJT05]. Density is described as an 11th order polynomial that represents the probability that any given pixel is bone. The polynomial is then normalized, between 1 and 0, and a probability image is computed for each CT slice. Image gradient is the second feature given in [SKJT05], and is derived from the following equation, where X and Y are the pixel locations of the image and G represents the image gradient at location XY in the dataset:

$$X = \frac{V(i+1,j) - V(i-1,j)}{dist(i+1,i-1)}, Y = \frac{V(i,j+1) - V(i,j-1)}{dist(j+1,j-1)} \tag{2.1}$$

$$G(i,j) = \sqrt{X^2 + Y^2}$$

Gradient determines density changes, where bones are higher intensities. Fitting an 11th order polynomial to Equation 2.2, where the probability of the bone surface given the knowledge of a particular feature [JT04], and $P(S) = P(\bar{S}) = 0.5$, with a

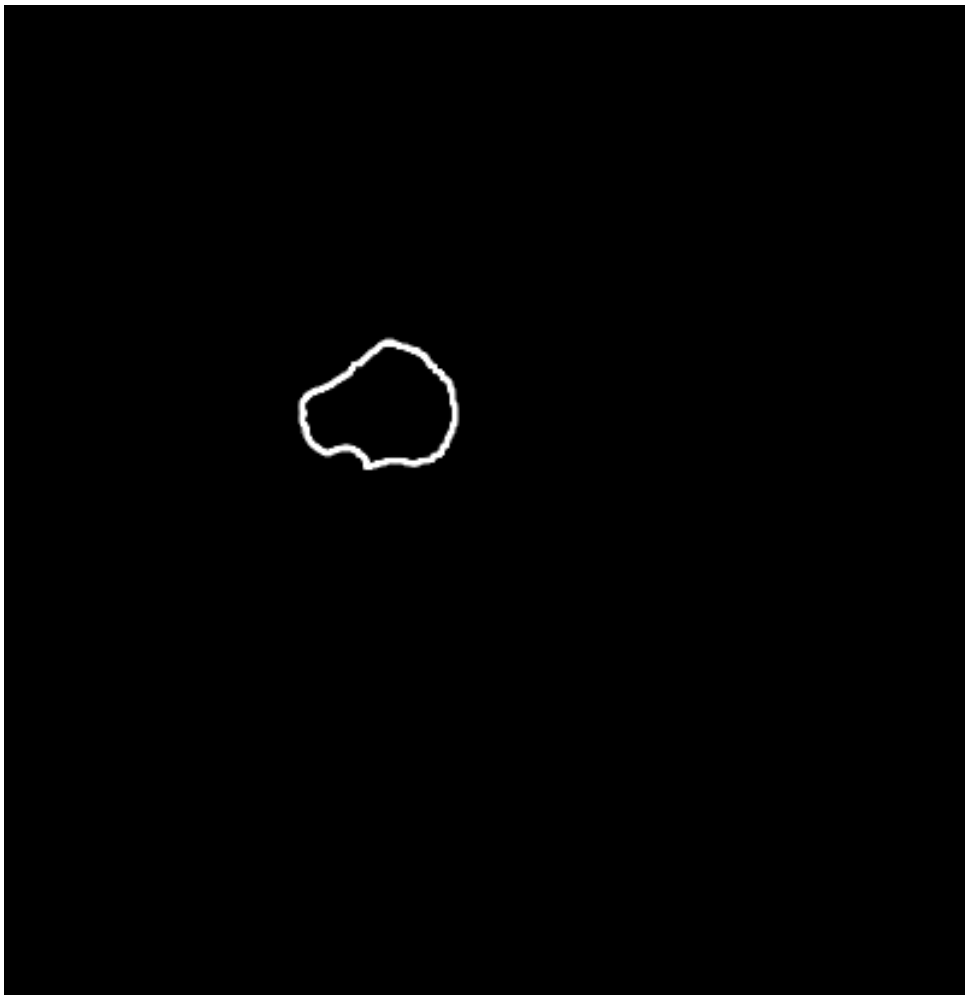

Figure 2.9: An example of Feature 1, density, applied to a CT slice.

range of 20 to 1134, gives us a result seen in Figure 2.13.

$$P(S|F) = \frac{P(F|S)P(S)}{P(F|S)P(S) + P(F|\bar{S})P(\bar{S})} = \frac{P(F|S)}{P(F|\bar{S}) + P(F|\bar{S})} \tag{2.2}$$

Canny edge detection is the most determining of the features by capturing approximately 96% of all edge points if a smoothing filter is applied to the image after edge detection.

The final features, energy absorption and first impact, function in a similar manner. These features traverse the image from all four sides, left to right, top to bottom

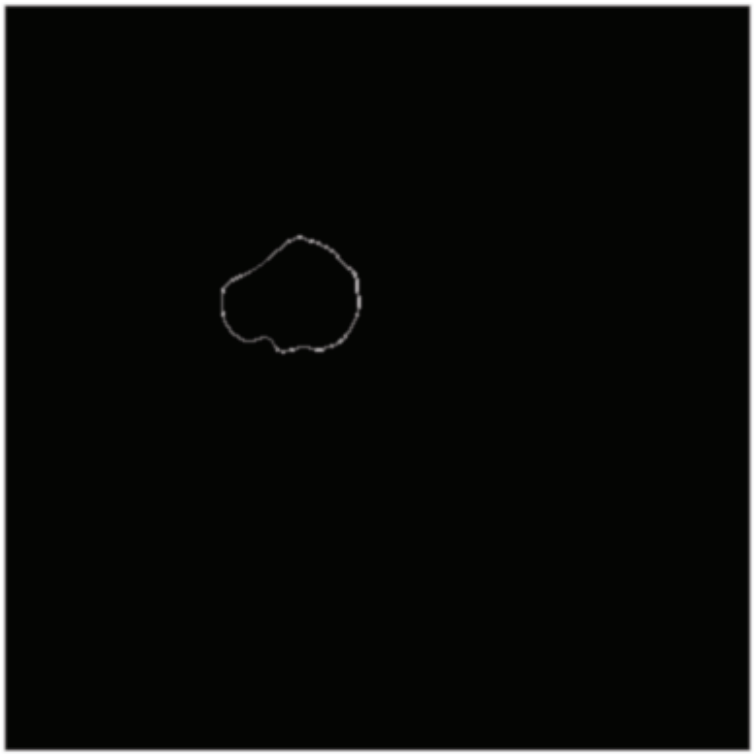

Figure 2.10: An example of Feature 2; Gradient applied to a CT image.

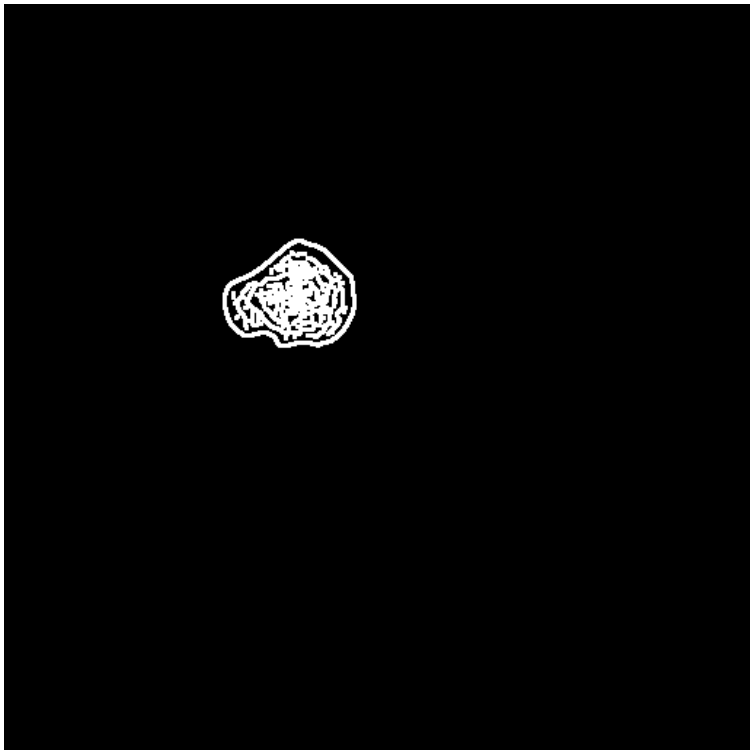

Figure 2.11: The same CT image with Canny edge detect applied to it.

and vice versa, and apply the following equation:

$$EA(i,j) = \begin{cases} 0.005(remaingEnergy) & \text{if D(i,j)} < 0.39\text{(MaxD)} \\ (D(i,j)/MaxD) & \text{if D(i,j)} \geq 0.39\text{(MaxD)} \end{cases} \quad (2.3)$$

where MaxD is the largest value in the given image [SKJT05]. First impact mimics the behavior of energy, in this case Xray, traveling through a medium. After the image is convolved with a 3x3 averaging filter, an 8th degree polynomial is created. First impact similarly navigates the rows and columns of the image until the first non-zero value is encountered in an aggressively thresholded image.

All features are then collected together using Equation 2.3 and a final segmentation is given.

The Bayes classifier, which combines the aforementioned features, is defined as:

$$P(S|F_{1,2,\ldots i,i+1}) = \frac{P(S|F_{1,2,\ldots,i})P(S|F_{i+1})}{P(S|F_{1,2,\ldots,i})P(S|F_{i+1}) + (1 - P(S|F_{1,2,\ldots,i}))(1 - P(S|F_{i+1})} \quad (2.4)$$

Combining the features in this manner gives us a result similar to that shown in Figure 2.14. This result will be used in Chapter 4 to determine which of the segmentation techniques works best in conjunction with the registration techniques discussed. These registration techniques will be discussed in the following chapter.

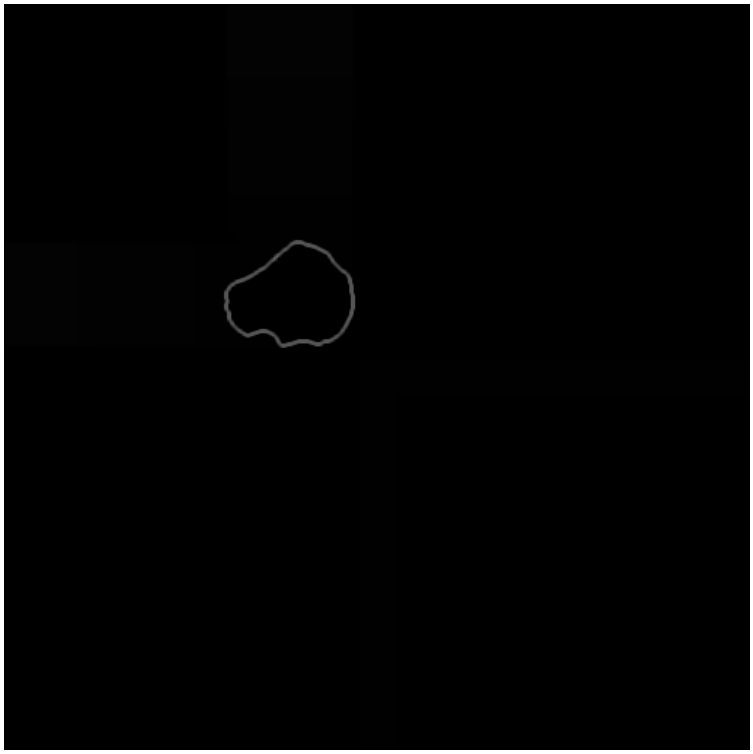

Figure 2.12: An example showing the result of the first impact feature.

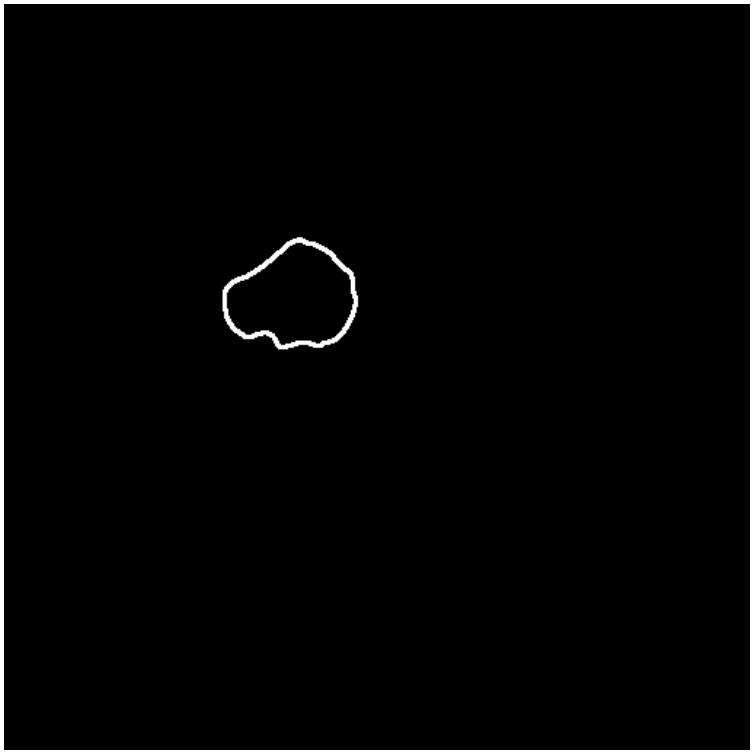

Figure 2.13: The energy absorbtion feature is shown on a slice of the CT phantom scaphoid scan.

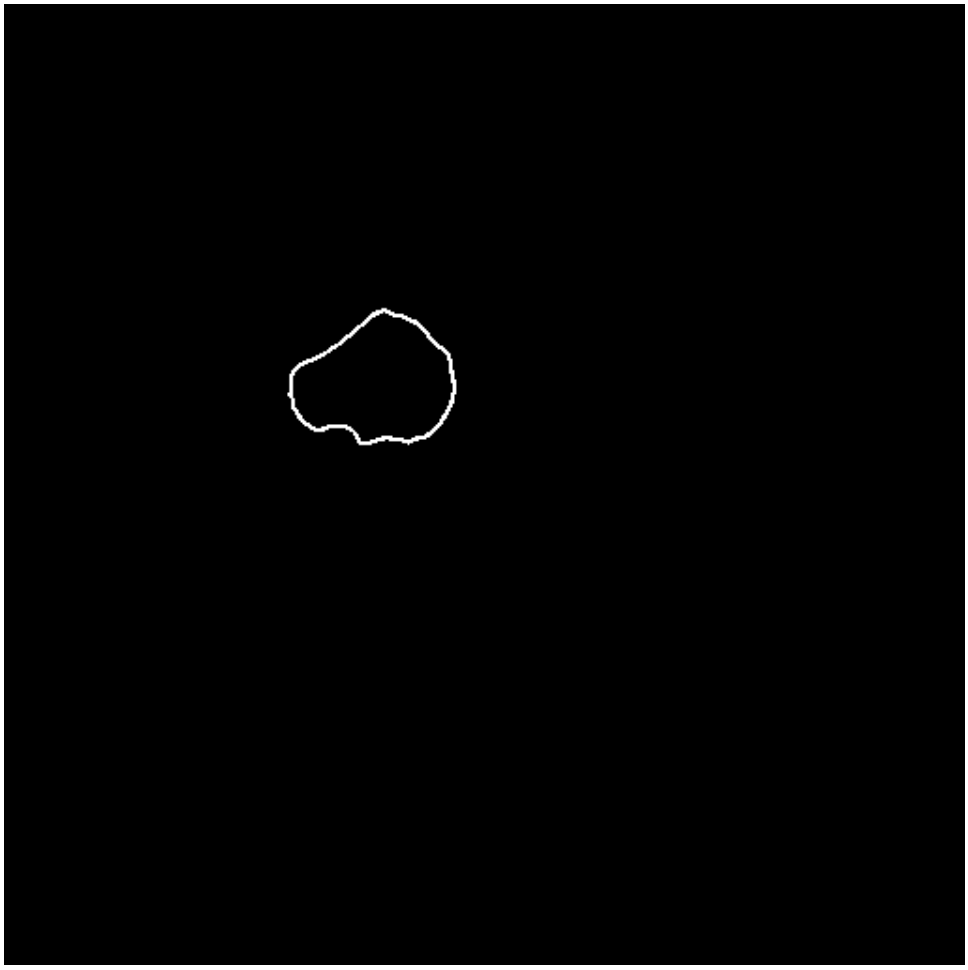

Figure 2.14: The final resulting fully segmented CT image slice.

Chapter 3

Registration

The main purpose of this thesis is to find a clinically acceptable mapping of two image modalities to one another. To perform a minimally invasive percutaneous wrist surgery, a surgery which requires the surgeon to have a graphical 2D or 3D representation of the anatomy on which he or she is working, a method by which the surgeon can monitor his or her progress is required. The two image modalities being used are CT; which represents the visual image (either 2D slices or a 3D model) the surgeon sees, and a set of ultrasound images; that provide the updating information of the surgery in real time. The problem of registering (mapping) these two image modalities together may seem to be an intuitive step. However, for a computer program to accomplish this task is much less simple. Computers are not designed to be intuitive machines. The task of aligning two images in its most simple terms, would be an exhaustive search in which each different orientation of the images would need to be calculated. After such a calculation was performed, the best match would be the result containing the lowest calculated error. To do this would require far more time than is available during a surgery. Therefore, a more intelligent approach is needed to

register the two data sets. Unfortunately, there are difficulties with the registration methods put forth and examined in this chapter that are discussed in greater detail for the Iterative Closest Point and Unscented Kalman Filter registration types.

To cover the topic of registration fully, one needs to premise their discussion with a general explanation of what it means to register two data sets to each other, and what the purpose of this process is. In the context of this research, "to bring two images acquired of the same anatomical subject in spatial alignment" [MV98] we heavily rely upon a foundational definition of what the goal of registration should be considered. The result of the registration we are striving for is a transformation, consisting of a translation vector and a rotation, which when applied to the moving data set will place the two sets on top of each other.

What is often viewed as the simplest way of registering the scaphoid involves using markers on the bone, which can be tacked in a process known as fiducial based registration. However, this type of registration is unusable with our application of percutaneous pinning of the scaphoid as the invasive procedure of applying screw mounted markers defeats the purpose of having a minimally invasive surgery. In addition, due to the small size of the scaphoid and the fact that the purpose of the surgery is to repair a fractured bone, there is not enough physical area on the bone to allow the placement of fiducial markers. Furthermore, adding any sort of screw to a bone which is as fragile as the scaphoid, would most likely result in further damage and possibly impede the already slow healing process discussed in Sections 1.2 and 1.3. These complications limit the method of registration to the intrinsic variety: either landmark based or segmentation based.

Intrinsic registration is a mapping that relies on the content of the images. In

the present context, CT and ultrasound, where no outside information is needed. By attaching a tracking device to the ultrasound transducer, each ultrasound image can be coupled with a file that contains the orientation and position of the transducers at the time the image was acquired. This allows one to build the individual ultrasound slices into a 3D model from segmented images [Che05]. Therefore, the primary registration techniques examined in this thesis are Iterative Closest Point, and Unscented Kalman Filtering. ICP is widely known and is used as an algorithm for registration while providing the golden standard. UKF is a newer registration method that has the potential to outperform ICP in capture range and execution time, and is discussed in Section 3.3.

3.1 Registration Background

Registration can simply be defined as the process where one data set, in this case a rigid body, is transformed from its original location in space to its correct corresponding orientation on another data set. This method relies upon the assumption that the two data sets are rigid bodies, thereby allowing the transformation that maps the moving data set to the fixed set to consist of a translation T, and a rotation R. If the two bodies were not rigid, a deformation value of the moving set would also have to be calculated. Registration can be as simple as using an interface to manually align the corresponding points using landmarks that are visible in both data sets, or using an automatic process such as Iterative Closest Point (hereinafter ICP) [BM] [Yan] or Unscented Kalman Filter (hereinafter UKF) [HA06].

3.1.1 Registration - Manual

Manual registration, as the name suggests, is a technique where the CT and ultrasound data sets are brought into alignment by the user. Once the two data sets are aligned properly, the resulting transformation, or the one that maps the two sets together, is found. Manually aligning the two sets is a slow process as there are three rotational and three translational parameters that all require aligning. This method is often the initial step in automatic registration due to most automatic registration techniques requirement of having a close initial starting position. In some circumstances, a manual registration can be close enough to facilitate the needs of a user. An example of a manual registration program can be seen in Figure 3.1.

3.1.2 Registration - Statistical Shape Model

A completely different approach to surface matching is described by F.M. Vos et al. who used a technique they referred to as "Statistical Shape Model without Using Landmarks" [VdBA+04]. Landmark based registration techniques require that a user select landmark points by hand, therefore these techniques tends to be error prone and tedious. Also, many bones are similar to the scaphoid insofar as they are quite smooth and featureless (shown in Figure 3.2), making it even more difficult to choose reliable landmarks.

The research contained within this article introduces a method which is applicable to any problem where explicit shape features are not easily identifiable. This technique is an adaption of the ICP and is applied to carpal bones. The results of this algorithm are quite impressive as seen in Figure 3.3 [VdBA+04]. The point to surface correspondence is much faster at converging to 100% than the point to point

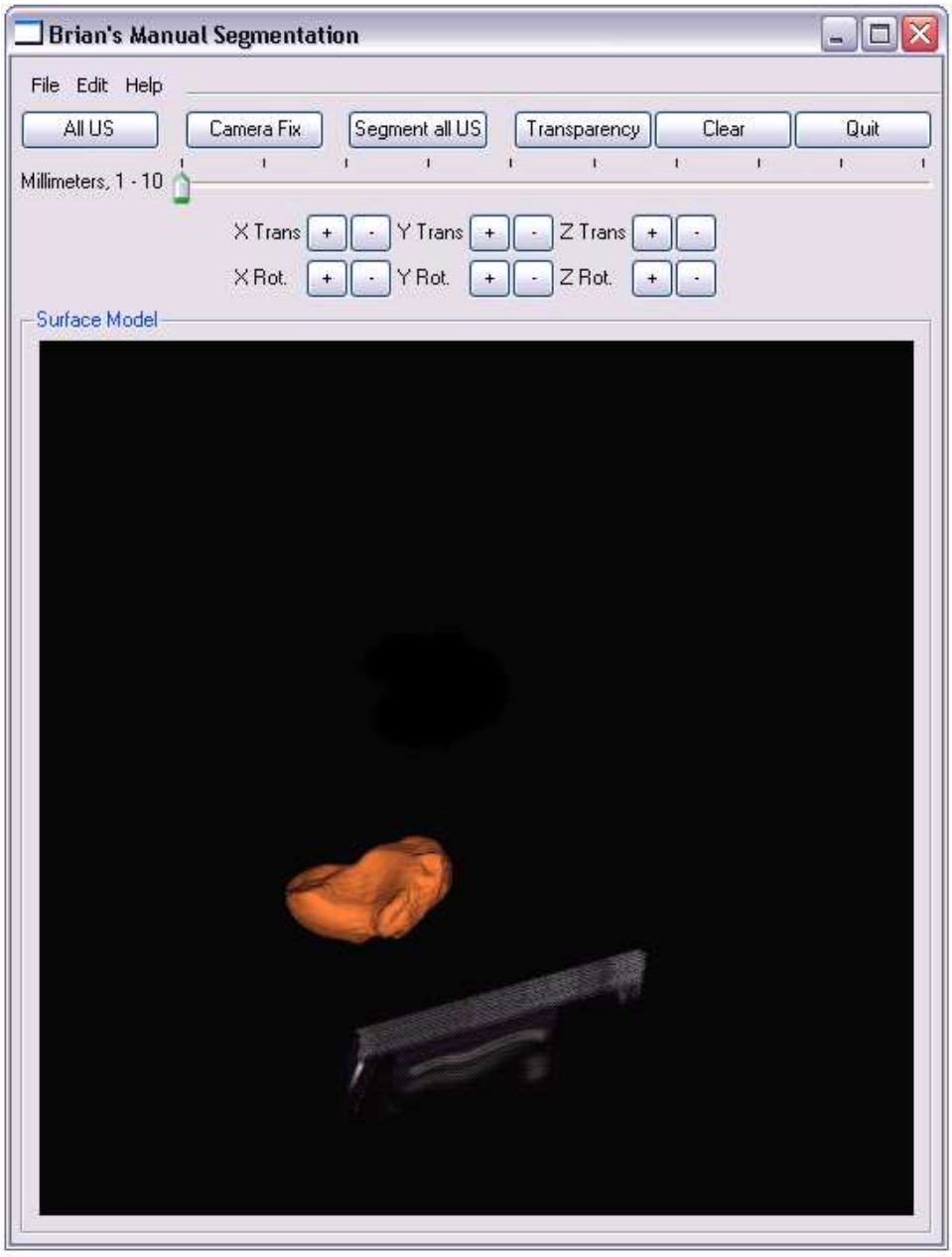

Figure 3.1: This shows the GUI which was implemented for this thesis. You can see it showing both the CT surface and the moving ultrasound data set.

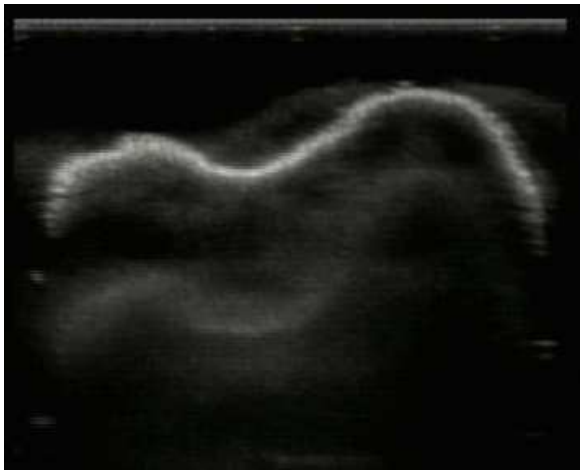

Figure 3.2: Notice the smooth surface, symmetry, and lack of destinguishing marks on the surface of the bone; this is an ultrasound scan of a scaphoid phantom.

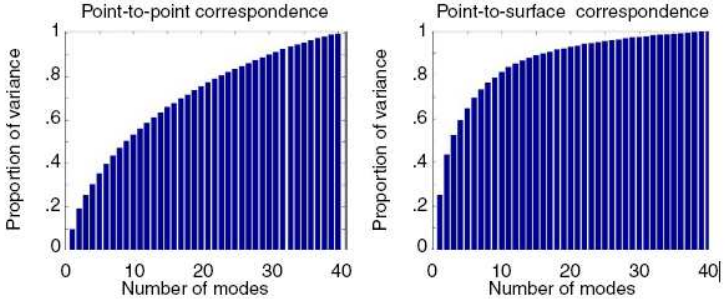

Figure 3.3: Figure taken from [VdBA+04] which shows the speed of convergence between point-to-point and point-to-surface registration.

correspondence. This approach could prove to work quite well with the scaphoid bone as its most predominate distinguishing feature is that it uses real data from patients, and not phantoms. While the process is applied to bones in the wrist that are almost featureless, it is nevertheless successful at segmenting most of the data set.

3.1.3 Registration - Maximum Intensity

Brendel et al. [BER+02] explain a registration method for registering 3D CT data and ultrasound imaging using an intensity based technique. The first part of the algorithm involves a surface estimation within the US image. As the visibility of bone surfaces depends on the direction of US propagation, the path of the probe is entered as a parameter for the surface estimation algorithm. Only when the path is known can the surface estimation be computed using a 3D CT data set. Once the virtual surface has been computed, the outline is overlaid in the US image, giving a proposed area in which to register. While this algorithm works very well, there is a large problem associated with the implementation involving the use of carpal US images. The scaphoid bone is a very smooth and symmetrical bone and the ones used by Brendal et al. in their study are located in the spinal column. These lumbar vertebrae have a very distinct shape with many points that can be used as landmarks. As discussed previously, this is not the case with the scaphoid bone as there are very few points to be used in land-marking. When using this technique, the time for registration, assuming the vertebrae are rigid in relation to each other, is 5-15s.

3.2 Iterative Closest Point

ICP [BM] has become the standard method employed to register two data sets to each other, and as it has been utilized for many years there are many variations of the ICP algorithm which either improve the reliability of the program or introduce time saving techniques to validate real-time or closer to real-time results [HA06]. The two papers discusse will be the original paper by Besl [BM] and a variation from Ziv

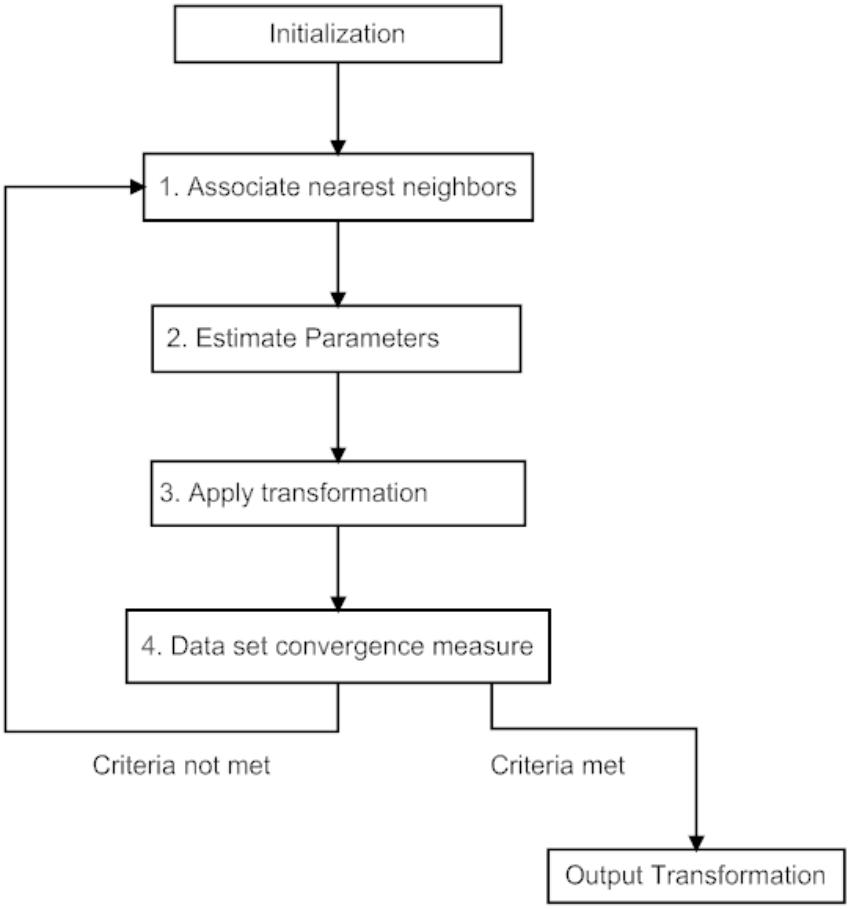

Figure 3.4: The ICP algorithm shown in four steps taken from [Yan]

Yaniv [Yan], which introduces k-D Trees in order to speed up the algorithm. The basic steps behind ICP are shown in Figure 3.4.

ICP offers a simplistic approach to a seemingly straight-forward problem. Intuitively, it seems a simple problem: take two clouds of points, match the points to each other, inspect the match, if it is not good enough shift closer until optimal results are achieved. This is much easier to do visually, even though it is more time consuming, than it being completed automatically.

A close initial alignment is required to avoid getting trapped in a local minimum (an incorrect registration). Getting trapped in a local minima, refereing to the minimization of the distance between corresponding points, can be detected by calculating the target registration error. A TRE value larger than a set margin means a registration may have failed, thus requiring a closer initial alignment to achieve better results. In the case of the scaphoid, due to its symmetry and small size, a very close initial alignment is required to avoid local minima.

In 1992, Paul Besl and Neil McKay published a paper introducing a novel way to register data sets to each other [BM]. Discussions outline various limitations of ICP by showing a study which employed ICP to register a femur bone to a permutated cloud of points disclosing some of the ICP's limitations. This study is the basis for using UKF over ICP as the gold standard within this thesis.

ICP has a strong dependence on the initial alignment of the data sets to each other. Tests demonstrate that the rotational component of the transformation has a much larger impact on the final registration error than the translational component. If the initial alignment is beyond ICP's capture range, there is a strong likelihood that the final registration will be "trapped in a local minima," as the algorithm is a minimization of Euclidian distance. The data set used for this thesis is of a scaphoid bone model, which is quite symmetrical, therefore the initial alignment dependency is quite high as due to its symmetry. ICP may provide a satisfactory minimization, but this can nevertheless result in an un-satisfactory registration if the algorithm registers to a local minima. Another issue that ICP struggles with is the strong influence from outliers due to the quadratic formation of the least squares cost function [Pet05]. All these factors considered, given a good initial alignment, ICP should perform well and

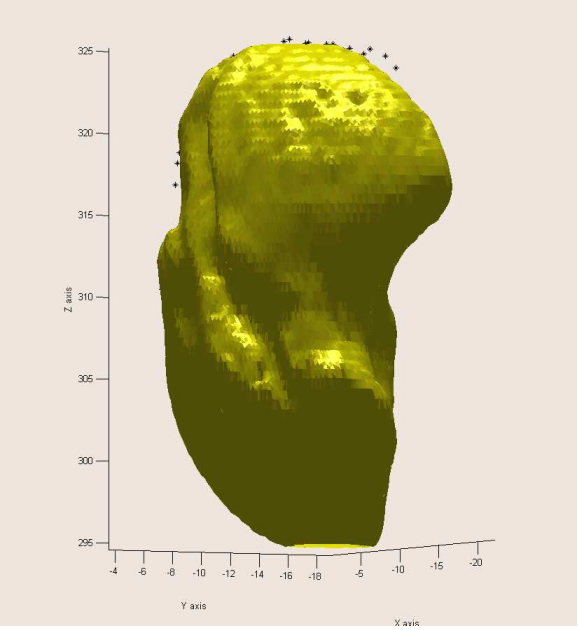

Figure 3.5: The end result of two tomographic data sets that have been successfully registered to each other.

result in a quick and accurate registration.

In addition to [BM], there are many different variants that exist [Yan] [MF93] [RL01] and each offers their own enhancements to the original implementation. Variants of ICP can modify the method used to store the points in forms that include K-D trees or increase speed by utilizing dynamic caching. There are also different model sampling algorithms that increase speed by minimizing the number of points selected from the point clouds. In order to make ICP more resistant to local minimas there are techniques including: removal of outliers, stochastic ICP, simulated annealing, and weighting of points [Hal06]. The variant of ICP employed to compute the results shown in Chapter 4 is one that uses a K-D tree representation of points to run more efficiently. This gives a better run-time performance than the base ICP in [BM], while still offering the same registration results.

3.3 Unscented Kalman Filtering

Unscented Kalman Filter [HA06]-based rigid-body point-based registration, proposed by Moghari and Abolmaesumi, is the most recent variant of the original ICP technique. As shown in [PT97], the algorithm extends the capture range of ICP and has a greater ability to address outliers than the original ICP technique. Moghari and Abolmaesumi also also state that there is a confidence measure which is calculated during the registration process and allows a user to see how quickly the registration is occurring and also provides a means by which to halt the registration when a pre-determined confidence measure is reached. In addition, since the UKF-based registration method is an incrementally processed registration, it has the possibility for real-time registration, which would make it a prime subject for use in the OR. There are claims made by Moghari and Abolmaesumi which state that the proposed UKF registration will outperform ICP in terms of complexity, capture range, execution, and final registration accuracy. This claim will be tested as ICP and UKF are run on identical data sets in identical situations, with results to follow in the following Chapter 4.

The following equations help explain the UKF algorithm as shown in Figure 3.6[1].

1. Shown in Equation 3.1 is the calculation of; the state vector $\hat{x}_i^-$ which is defined as a 6x1 vector which contains the registration parameters, and $P_{\hat{x}_i^-}$ where P is the covariance matrix from the state model.

$$\hat{x}_i^- = \hat{x}_{i-1}, P_{\hat{x}_i^-} = P_{\hat{x}_{i-1}} + \sum Q \tag{3.1}$$

2. A new point i is then appended to the existing data set where; $\hat{y}_{1:i}$ is the next

[1]The equations 3.1 - 3.4 have been taken from [HA06] and are used with permission from Mehdi Hedjazi Moghari.

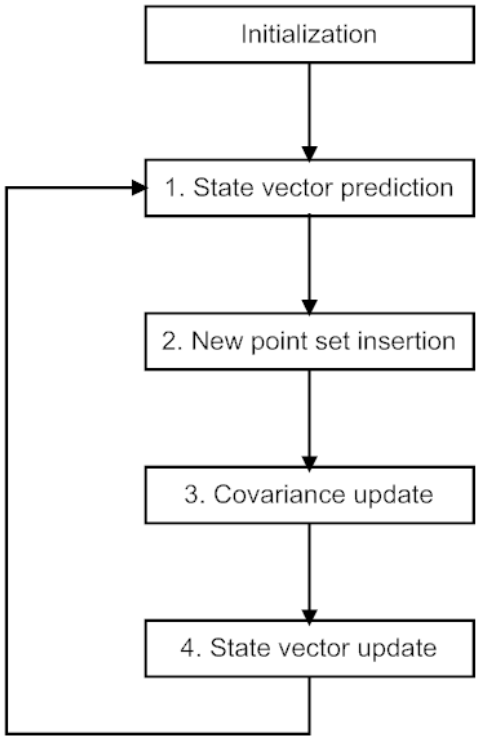

Figure 3.6: The flowchart from page 6 of [HA06] which shows the steps used in calculating a registration using UKF.

point added, $\mathbf{R}$ is the rotational component and $\mathbf{t}$ is the translational component of the i^{th} point.

$$\hat{y}_{1:i} = R_{(\hat{\theta}_x, \hat{\theta}_y, \hat{\theta}_z)} u_{1:i} + t_{(\hat{t}_x, \hat{t}_y, \hat{t}_z)} \tag{3.2}$$

3. Update the covariance matrix $\mathbf{P}$.

$$P_{\hat{x}_i} = P_{\hat{x}_i^-} - K_{1:i} E[y_{1:i} y_{1:i}^T] K_{1:i}^T \tag{3.3}$$

4. Update the state vector $\hat{x}^i$ in the corresponding points in the data set ($y_{1:i} - \hat{y}_{1:i}$). If there is a point i+1 then repeat the process by adding another point, i+1 tothe existing data set.

$$\hat{x}^i = \hat{x}_i^- + K_{1:i}(y_{1:i} - \hat{y}_{1:i}), \tag{3.4}$$

Chapter 4

Experiments and Results

Registration and segmentation methods discussed in previous chapters are now used to compare the accuracy and speed of the Iterative Closest Point [BM] and Unscented Kalman Filter base Registration techniques [PT97] [HA06]. In order to allow for unbiased testing, all experiments were run on the same machine, on identical data sets, with each data set being configured with 500 unique initial alignments. In addition to testing ICP against UKF in the experiments below, secondary testing is also done as the different data sets used are derived from the same original data which was segmented utilizing different segmentation algorithms. The first segmentation used is one discussed in [JT04] and reviewed in Chapter 2, which uses a Bayesian Probabilistic Framework (FAPBED) to extract the bone surface from within the US band. The second being an approach which is discussed in [Pet05] and has its outline shown in Figure 4.1 which assumes the bone's surface response to be on the surface of the ultrasound response.

Since the latter approach does not take into account properties of ultrasound images, the expectation is that the segmentation method from [JT04] will provide a

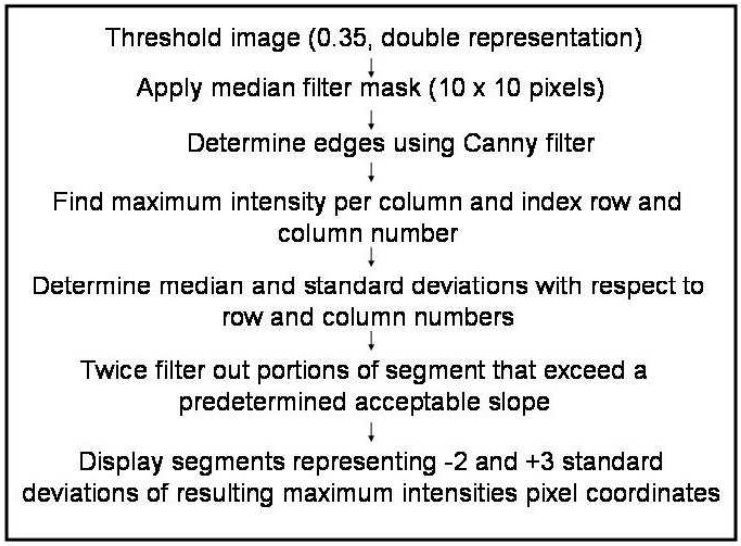

Figure 4.1: Explanation of naive segmentation used in second experiment data set.

closer representation of the actual bone's surface, resulting in a more favorable final registration. In addition, since these experiments are investigating the registration accuracy of ICP against UKF, the objective of these experiments is to see if UKF can outperform ICP in terms of initial capture range, run-time of registration, and a final registration with a lower target registration error [Hed].

4.1 Experiments

There are four different types of tests run that accumulate data to determine support for UKF being used over ICP, and a Bayesian Framework segmentation having a higher accuracy than a naive segmentation. The four experiment types are: I. An ICP registration of a naively segmented ultrasound data set to a CT volume, II. An ICP registration utilizing a Bayesian segmented data set, III. A UKF registration using the same ultrasound data set as in experiment I., IV. A UKF registration of the ultrasound

data used in II. Each of these tests were run for a total of 500 iterations, where each iteration consists of a completed registration occurring, each iteration with a different initial alignment. To expand the validity of these experiments, there were three initial capture ranges run for each UKF and ICP to provide insight into the increased capture range provided by employing UKF for registration. These capture ranges include applying a random transformation of ± 0.5mm with a rotational disturbance of ± 0.5 degree for a number of 500 trails per data set (manually and Bayesian segmented data). These experiments are then repeated for random transformations in the range ± 0.5mm and ± 0.5 degrees, ± 1.5mm and ± 1.5 degrees, and finally ± 5.0mm to ± 5.0 degrees.

By calculating the error of the final registration of each experiment in terms of TRE, we can determine if the performed registration was successful. It is assumed within this thesis that a successful registration is one that has an average TRE (averaged across the x, y, and z axis) of less than 2mm and 2 degrees; values that have been shown as a successful registration in [Hed]. Since it has already been shown that both ICP [BM] and UKF [HA06] have the ability to be accurate to within 1.5mm and 1.5degree errors along each axis. It is also known that the symmetry of the scaphoid bone, of which all the test data sets are comprised, along the z-axis, will cause the error in the z-direction to be higher than the x, and y-axes. Therefore, it can be assumed that the ability of the respective registration algorithms to align the data sets is not in question. Results of the experiment will be shown in the tables used to compare the algorithms.

4.1.1 Data used in Experiments

There are three different data sets used in the aforementioned experiments, these are: a CT mesh of an artificial scaphoid bone, an array of 300 ultrasound images segmented using the Bayesian segmentation algorithm discussed in [JT04], and a similar ultrasound data set from the same original data but segmented using the segmentation from [Pet05]; see Figure 4.1.

The CT images that were used were acquired using a GE LightSpeed scanner with an in plane resolution of 0.188mm x 0.188mm with 1.25 mm between slices. [BALP06] The ultrasound data was taken by fully submerging the scaphoid analogs (phantoms) in a water bath. Then, using a pre-calibrated US probe, as discussed in [Che05], images were captured using frame grabbing software, creating a series of US images. The images also had corresponding data that demonstrated the orientation of the US probe in relation to the phantom bone. This data was captured by tracking the DRB on the transducer as shown in Figure 4.2 in relation to the DRB attached to the phantom rig. According to the experiments done in [ACEP05] the US data acquired using the aforementioned rig, an accuracy of 0.64 mm, which is well within the requirement of sub 2mm error for use in the OR.

The ultrasound data sets are read in by the two registration algorithms; 30 points along the bones surface are chosen at random from each slice. The points from each slice are then combined into a set of points that are placed into correct spatial position according to the respective slice orientations during image acquisition. This creates a second surface to register to the CT surface mesh. The two surfaces are then aligned using a pre-computed transformation calculated in [HA06], which places them in an ideally aligned position. It is from this initial alignment that the random disturbances

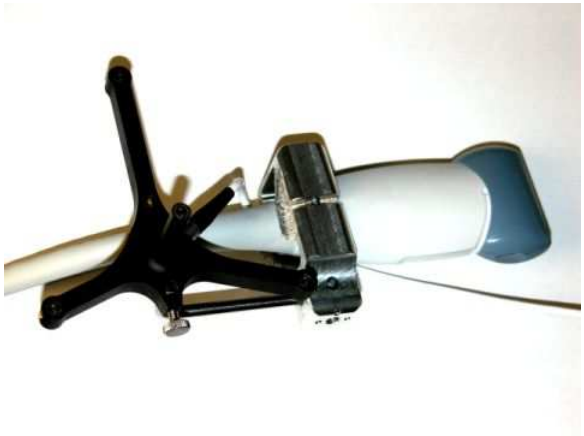

Figure 4.2: The image shows the ultrasound transducer with a DRB tracking device which was used to capture the images used in this thesis.

within given ranges are applied. The CT mesh in use is one that is used in tests in [Pet05] and [HA06]. Ultrasound images were also captured from the same artificial scaphoid bone used to generate the CT mesh surface. The surface was extracted from the original CT scan through the use of "Mesher," discussed in Chapter 2. The segmented CT volume is considered to represent a perfectly segmented scaphoid bone.

4.2 Experiment Results

The results from the simulations have been tabulated below, and will be discussed to determine if they confirm that UKF will out perform ICP in terms of initial capture range, run-time of registration, and a final registration with a lower target registration error. The tables have been divided to show the results in logical order, and since the main focus of the thesis was to determine which of ICP or UKF algorithms are more accurate over a wide range of initial alignments, the tables show the results for ICP and UKF in the different ranges mentioned above. There was a secondary emphasis

on the method used to segment the data and this was the manual naive approach or the feature-based Bayesian framework technique from [JT04]. The tables below, show the mean error, median error and the Standard Deviation. The second row from the bottom shows the percentage of trials from each experiment resulting in an accuracy of less than 2.0mm; as discussed above, this is the limit that formulates a successful registration. The bottom row shows the run-time of the algorithm to help show the validity of the algorithm in terms of real-time implementation.

The error in these experiments is calculated by taking the TRE on ten points from pre-measured fiducial points, taken from previous studies, which are the gold standard from the data sets in use. The ten fiducial points have the final registration applied to them, then the Euclidian distance and the rotational error are computed giving the final error. These errors are stored in an array and read into MATLAB using a program which then computes the mean, median and standard deviation. By running a filter on the array that counts the number of trials having an accuracy closer than 2.0mm and 2 degrees, the percentage of successful registrations is computed.

Table 4.1: Experiment Results: Error for $\pm 0.5mm \pm 0.5deg$

	$ICPManual$	$ICPBayes$	$UKFManual$	$UKFBayes$
Mean Error	25.23	11.39	2.51	1.22
Median Error	0.20	0.18	2.36	1.09
Stan Dev of Errors	25672	10894	0.80	0.56
% successful	98.2%	98.6%	85.4%	90.8%
Computation Time	26.0hrs	25.0hrs	35min	38min

The results of the first experiment, see Table 4.1, show findings that the average error across all the trials, except for for the manually segmented UKF experiment, are within 2.0mm accuracy and could be used in clinical applications. Also since the standard deviations for this test are lower for the ICP algorithm, this supports

the claims made in [HA06] that with a close initial alignment ICP has the capability of performing an accurate registration. And while ICP seems to be outperforming UKF, the results of UKF are still well within the limits which provide useful and accurate registration results. The experiments using the manually segmented data have a higher error rate which stands to suggest that the feature-based segmentation is providing a more exact representation of the bone's surface within the ultrasound's response band. This is also confirmed in the ICP trial where the error is lower on the data sets comprised of the feature-based data. In addition to the registration error, one must also notice the computation time. ICP took approximately 25 hours to compute the 500 trials on the data mentioned above for each of the manual and Bayes segmented data sets. The run-time of the UKF algorithm was, by stark contrast, approx 25 minutes on the same 500 registrations. This goes to show that the accuracy of the ICP algorithm is a result of a much more tedious and computationally intensive process. The UKF algorithm has failed to outperform the ICP algorithm in in this simulation, in terms of accuracy.

Table 4.2: Experiment Results: Error for $\pm 1.5mm \pm 1.5deg$

	$ICPManual$	$ICPBayes$	$UKFManual$	$UKFBayes$
Mean Error	441.86	481.44	6.86	5.22
Median Error	0.22	0.20	2.39	1.11
Stan Dev of Errors	85826	97562	21.20	20.92
% successful	57.6%	61.8%	81.8%	87.4%
Computation Time	29hrs	29hrs	16hrs	14hrs

This simulation, see Table 4.2, shows a more favorable result to the UKF algorithm. Where the ICP results are showing a mean result of 25.23mm there is still a median error of 0.20mm for the manually segmented data. This shows that in data sets having an initial alignment off by only 0.5mm and 0.5 degrees there is a chance of

the final registration being trapped in a local minima. However, the UKF algorithm shows a much lower standard deviation than ICP using both data sets. We also see that the ultrasound data segmented using the technique in [JT04] is registered with a much lower error than the manually segmented one. This shows that by using the technique provided in [JT04] one can achieve a much more accurate alignment. This simulation also shows the ability of the UKF based registration to avoid becoming trapped in a local minima.

Table 4.3: Experiment Results: Error for $\pm 5.0mm \pm 5.0deg$

	$ICPManual$	$ICPBayes$	$UKFManual$	$UKFBayes$
Mean Error	1094.00	994.93	30.74	26.90
Median Error	56563	56563	2.74	1.33
Stan Dev of Errors	1.14×10^3	1.10×10^3	49.80	47.88
% successful	13.2%	12.6%	31.2%	69.4%
Computation Time	33hrs	34hrs	16hrs	13hrs

The final Table 4.3 one can now see the simulations which show an initial alignment for the ultrasound data sets greater than 1.5mm and 1.5 degrees from the proper alignment, and as expected we see the larger capture range of the UKF-based program becoming very apparent. Even, with the probabilistically segmented, data sets that had initial alignments perturbed by as much as 5.0mm and 5.0 degrees the UKF-based registration able to accurately register over half of the trials. ICP no longer has the capacity to correctly register at this point as is noted by the soaring error and standard deviation values that are shown above.

Chapter 5

Conclusions and Future Work

5.1 Conclusion

In this thesis, we investigated the performance of two feature-based registration techniques to align ultrasound and CT data sets. The results demonstrate that a combination of the Unscented Kalman Filter (UKF) and a Bayesian segmentation of ultrasound data leads to the lowest target registration error between the corresponding landmarks in the two data sets.

From Chapter 4's experimental data we are able to infer that the initial alignment, especially in terms of the rotational component, is a key determining factor in the success of ICP. Moghari and Abolmaesumi claim that UKF on the other hand has a capture range that exceeds that of ICP [HA06] and this is apparent from the results shown in Tables 4.1 to 4.3. Also shown in Chapter 4 is the stronger performance of the ultrasound data that has been segmented with the method discussed in [JT04]. In every case when it is compared to the manual segmentation the feature-based segmentation outperforms the other segmentation meaning it is a much more

accurate representation of the bone's surface within the ultrasound scans. By utilizing this knowledge we can see by simply varying the approach used to compose the experimental data we can achieve greater accuracy in all registrations performed.

Unfortunately, the results of the experiments did not provide the unanimous results that were expected: that UKF will outperform ICP in all experiments. In closer initial alignments it was expected that the UKF algorithm would outperform ICP which it did not, at least in terms of accuracy. In every simulation run the UKF registration process ran hours faster than the ICP registration on the same machine. However, it should be noted that accuracy, not computation time, was the metric for the experiments above. When the initial alignments were moved past 0.5mm and 0.5 degrees from the ideal registration, UKF started to show its strong ability to register data with a further initial alignment than ICP. As the distance of the initial alignment increased, UKF returned a stronger final alignment than ICP in all experiments showing that it is a strong competitor for ICP in future experiments.

5.2 Future Work

The experiments above show that UKF is a strong contender for use in the operating room for CAS. The experiments above are not enough to prove this as they were performed were on phantom data, meaning that it is an accurate anatomical model for the scaphoid but under ideal conditions. There is no extra interference from skin and muscle tissue as there would be in an actual human wrist ultrasound scan. In addition, the phantom data shows only one bone, the scaphoid, when in reality there are 8 bones in the wrist. This means there will be an additional strong response from those bones in an ultrasound scan. The feature-based segmentation algorithm from [JT04] has the

capability to segment those bones as well as the scaphoid so further experiments on actual human data can be performed. By testing on human data we can bring the use of UKF one step closer to the operating room for minimally invasive surgery where it will have the ability to help many people suffering from fractured scaphoid bones and not wanting to go into open surgery for which the recovery time is approximately 8 weeks. This thesis is but one step into the investigation of utilizing the Unscented Kalman Filter registration technique in medical applications.

The visualization tool which was developed for this research could also be improved upon as the initial use for this program was to be a preliminary segmentation method for ultrasound images in order to aid the actual segmentation step. The user would use the X, Y, and Z translational and rotational buttons to align the two data sets with each other, essentially registering them manually, and then deleting all the data in the individual ultrasound slices which is more than a threshold distance from any intersection between the CT surface mesh and the ultrasound images. There was a complication using VTK to relocation the origin of a volume to the center mass of an object, none of the available methods would properly center the origin into the "middle" of the volume. This caused the rotation of the data set to be more difficult, as figuring out how to move the origin inside of the mesh would make rotations more intuitive. There are also buttons which allow for a change in the transparency of the data to allow the user to see hidden spots and how well they are aligned with each other. Lastly there is a button which allows the user to zoom in on the displayed data in order to maximize the visibility of the region of interest.

As mentioned there are some limitations to what the software can currently do with the ultrasound slices and CT. There is an incomplete function, mainly the one

which segments the ultrasound, which is due to a change in focus of the thesis. Currently the code is about 80% complete to do the segmentation which works by looking for all the locations in the space which ultrasound and CT sets intersect. At all points where intersections occur it can be assumed that there is bone surface in the ultrasound slice so all data in the ultrasound image that is within three pixels (for example) in all directions can be used as the new "segmented image." It would also be useful to include a feature that does a TRE measurement to determine the accuracy of the current alignment. Depending however on the size of the data sets it may not be feasible to calculate this measure, but some feedback on the accuracy would be a great help when fine tuning the alignment.

Bibliography

[AB94] R. Adams and L. Bischof. Seeded region growing. *IEEE Transactions on Pattern Analysis and Machine Intelligence*, 16(6):641–647, June 1994.

[ACEP05] P. Abolmaesumi, T. Chen, R. Ellis, and D. Pichora. A system for ultrasound-guided computer-assisted orthopaedic surgery. 2005.

[ALA01] L. Adolfsson, T. Lindau, and M. Arner. Acutrak screw fixation versus cast immobilization for undisplaced scaphoid wrist fractures. *Journal of Hand Surgery*, 26B:3:192–195, 2001.

[BALP06] M. Beek, P. Abolmaesumi, S. Luenam, and D. Pichora. Intra-operator variability for a new percutaneous scaphoid pinning procedure using ultrasound guidance. 2006.

[BER+02] B. Brendel, H. Ermert, A. Rick, M. Stockheim, and S. Winter. Registration of 3d ct and ultrasound datasets of the spine using bone structures. *Computer Aided Surgery*, pages 146–155, 2002.

[BM] P. J. Besl and N. D. McKay. A method for registration of 3-d shapes.

[BPA+05] M. Beek, C. Peters, P. Abolmaesumi, T. Chen, R. Sellens, and D. Pichora. Ultrasound guided scaphoid pinning. *CAOS*, pages 26–28, 2005.

[CBEP05] C.K. Chan, D. Barratt, P. Edwards, and G. Penny. Cadaver validation of the use of ultrasound for 3d model instantiation of bony anatomy in image guided orthopaedic surgery. *CAOS*, pages 26–28, 2005.

[Che05] T.K. Chen. Ultrasound guided computer-assisted orthopaedic surgery. *Master's thesis, Queen's University, Kingston, Ontario*, 2005.

[CTL+98] L. Carrat, J. Tonetti, S. Lavallee, P. Merloz, L. Pittet, and J. Chirossel. Percutaneous computer assisted iliosacral screwing: Clinical validation. *Miccai*, pages 84–91, 1998.

[CTMT00] L. Carrat, J. Tonetti, P. Merloz, and J. Troccaz. Percutaneous computer assisted iliosacral screwing: Clinical validation. 2000(1229-1237), 2000.

[FWD04] E.A. Firle, S. Wesarg, and C. Dold. Mutual information based registration for ultrasound and ct datasets. In *Proceedings of SPIE*, volume 5370, pages 1130–1138, 2004.

[HA06] M. M. Hedjazi and P. Abolmaesumi. A new point-based rigid-body registration algorithm based on unscented kalman filter. pages 1–18, 2006.

[Hal06] Y. Halchenko. Icp slides. *http://www.onerussian.com/classes/cis780/icp-slides.pdf*, pages 6–7, 2006.

[HDM+98] J. L. Herring, B. M. Dawant, C. R. Maurer, D. M. Murator, R. L. Galloway, and J. M. Fitzpatrick. Surface-based registration of ct imagages to physical space for image-guided surgery of the spine: A sensitivity study. *IEEE Transactions on Medical Imaging*, 17-5:743–753, 1998.

[Hed] M. Hedjazi. Target registration error estimation in the presence of anisotrpic additive gaussian noise.

[JT04] A. K. Jain and R. H. Taylor. Understanding bone responses in b-mode ultrasound images and automatic bone surface extraction using a bayesian probabilistic framework. 5373:131–142, 2004.

[LC87] W. E. Lorensen and H. E. Cline. A high resolution 3d surface construction algorithm. In *SIGGRAPH '89: Proceedings of the 14th Annual Conference in Computer Science*, pages 163–169, 1987.

[ME04] B. Ma and R. Ellis. Surface-based registration with a particle filter. *MICCAI 2004*, pages 566–573, 2004.

[MF93] Calvin R. Jr Maurer and J. Micheal Fitzpatrick. A review of medical image registration. *Interactive Image-Guided Neurosurgery*, pages 1–49, 1993.

[MH03] V.L. Moser and H. Krimmerv T.J. Herber. Minimal invasive treatment for scaphoid fractures using the cannulated herbert screw system. *Techniques in Hand and Upper Extremity Surgery*, pages 141–146, 2003.

[MV98] J. B. Maintz and M. A. Viergever. A survey of medical image registration. *Medical Image Alaysis*, March 1998.

[Pet05] C. Peters. Percutaneous pinning of non-displaced fractured scaphoids using ultrasonography. *Master's thesis, Queen's University, Kingston, Ontario*, 2005.

[PMV03] J. P. W. Pluim, J. B. A. Maintz, and M. A. Viergever. Mutual-information-based registration of medical images: A survey. *IEEE Trasactions on Medical Imagine*, 22(8):986–1004, 2003.

[PT97] X. Pennec and J.P. Thrion. A frame work for uncertainty and validation of 3d registration methods based on points and frames. *Computer Vision*, 25-9:203–229, 1997.

[RL01] S. Rusinkiewicz and M. Levoy. Efficient variants of the icp algorithm. *Interactive Image-Guided Neurosurgery*, pages 145–152, 2001.

[RN03] MD R. Nishihara. The dilemmas of a scaphoid fracture: A difficult diagnosis for primary care physicians. *Hospital Physician*, pages 24–40, 2003.

[SKJT05] D. Scepanovic, J. Kirshtein, A. K. Jain, and R. H. Taylor. Fast algorithm for probabilistic bone edge detection (fapbed). In *Proceedings of SPIE*, volume 5747, pages 1753–1766, 2005.

[Sug03] N. Sugano. Computer-assisted orthopedic surgery. *Journal of Orthopaedic Science*, 8:442–448, 2003.

[TCB+01] J. Tonetti, M.D. L. Carrat, Ph.D. S. Blendea, M.D. P. Merloz, M.D. J. Troccaz, Ph.D. S. Lavalle, and M.D. J.P. Chirossel. Clinical results of percutaneous pelvic surgery. computer assisted surgery using ultrasound compared to standard fluoroscopy. *Computer Aided Surgery*, 6:204–211, 2001.

[TTR94] J. Trobaugh, D. Trobaugh, and W. Richard. Three-dimensional imaging with stereotactic ultrasonography. *Computerized Medical Imaging and Graphics*, 18:315–323, 1994.

[VdBA+04] F.M. Vos, P.W. de Bruin, G.M. Aubel, G.J. Streekstra, M. Maas, L.J. van Vliet, and A.M. Vossepoel. A statistical shape model without using landmarks. In *The 17th International Conference on Pattern Recognition*, pages 1–4, 2004.

[Yan] Z. Yaniv. Rigid registration: The iterative closest point algorithm.

[YWCS02] H.S.F. Yip, W.C. Wu, R.Y.P. Chang, and T.Y.C. So. Percutaneous cannulated screw fixation of acute scaphoid wrist fracture. *Journal of Hand Surgery*, 27B:42–46, 2002.